Microfluidic Quantitative Analysis Of Cellular Secretions Via Droplet Based Fluorescence Polarization Immunoassay With On-Chip Preconcentration

by

Colin Jennings

A dissertation submitted in partial fulfillment
of the requirements for the degree of
Doctor of Philosophy
(Chemistry)
in The University of Michigan
2012

Doctoral Committee:

Professor Michael D Morris, Chair
Professor Mark A Burns
Professor Nils G Walter
Emeritus Professor James O Wilkes

2012

To my friends and family

Acknowledgements

This dissertation would never have been possible without the support of numerous friends, colleagues and co-workers. I extend my deepest thanks to all those who helped me over the years; specifically, to the Kennedy Lab 'Affinity girls,' Brian Johnson, Dr Carlos Baiz and his wife Sarah Baiz, Evan Arthur, Jaesung Lee and countless others who helped me when I was most in need, I offer my eternal gratitude. Additionally, I would like to especially thank Dr Wilkes for his invaluable help in numerical modeling of fluidic systems, Dr Mark Burns for his patience and compassion, and Dr Michael Morris for agreeing to serve as my Chair.

Table of Contents

List of Figures

List of Appendices

List of Abbreviations and Symbols

•	Dot product
∇	Nabla (gradient)
Å	Angstrom
A	Area
aCSF	Artifical cerebral spinal fluid
Ar^+	Argon ion
BPE	Bipolar electrode
BSA	Bovine serum albumin
BSS	Balance salt solution
C	Concentration
$CaCl_2$	Calcium dichloride
CD-1	Cluster of differentiation 1
CE	Capillary electrophoresis
cm	Centimeter
CO_2	Carbon dioxide
D	Diffusion coefficient
D_H	Effective diameter of channel
DMSO	Dimethylsulfoxide

DNA	Deoxyribonucleic acid
dpi	Dots per square inch
e.g.	*Exempli gratia*
ECCD	Electron-multiplying charge coupled device
EDTA	Ethylenediaminetetraacetic acid
EFGF	Electric field gradient focusing
ELISA	Enzyme-linked immunosorbent assay
fM	Femptomolar
FPIA	Fluorescence polarization immunoassay
FRET	Förster resonance energy transfer
FTC	Fluorescein isothiocyanate
FTS	Trichloro(1H,1H,2H,2H-perfluorooctyl)silane
GOX	Glucose oxidase
H_2O_2	Hydrogen peroxide
H_2SO_4	Sulfuric acid
HCl	Hydrochloric acid
HF	Hydrofluoric acid
HMDS	Hexamethyldisilazane
HNO_3	Nitric acid
HPLC	High performance liquid chromatography
HRP	Horseradish peroxidase
Hz	Hertz
i.d.	Inner diameter

i.e.	*Id est*
ICP	Ion concentration polarization
IEF	Isoelectric focusing
IMR	Immunoreagent buffer
K_a	Affinity constant
KCl	Potassium chloride
kg	Kilogram
KH_2PO_4	Potassium phosphate
kV	Kilovolts
LC	Liquid chromatography
LIF	Laser induced fluorescence
LOD	Limit of detection
m	meter
M	Molar
$MgCl_2$	Magnesium dichloride
$MgSO_4$	Magnesium phosphate
min	Minute
mL	Millileter
mm	Millimeter
mM	Millimolar
mW	Milliwatt
MΩ	Megaohm
n	Number of replicates

Na_2HPO_4	Disodium phosphate
NaCl	Sodium chloride
NaH_2PO_4	Sodium phosphate
NaOH	Sodium hydroxide
NH_4OH	Ammonium hydroxide
nL	Nanoliter
nm	Nanometer
o.d.	Outer diameter
^oC	Degrees Celsius
OTCS	Octadecyltrichlorosilane
p	Negative logarithm
p	Pressure
P	Wetted perimeter
Pa	Pascal
PBS	Phosphate buffered saline
PCR	Polymerase chain reaction
PDMS	Polydimethylsiloxane
pM	Picomolar
pM	Picomolar
Q_o	Oil flow rate
Q_w	Aqueous flow rate
r	Fluorescence anisotropy
RFU	Relative fluorescence unit

RPMI	Roswell Park Memorial Institute
RSD	Relative standard deviation
s	Second
SEM	Standard error method
Si	Silicon
SPE	Solid phase extraction
t	Time
TGF	Temperature gradient focusing
UI	International unit (enzymatic activity)
UV	Ultraviolet
V	Volts
V	Volumetric flow rate
v/v	Volume per volume
Zn^{2+}	Zinc (II) ion
β	Beta
δ	Partial derivative
ε	Permittivity of media
κ	Ionic strength
μ	Viscosity
μm	Micrometer
μM	Micromolar
ρ	Density
φ	External electric potential

Φ	Total electric potential
Ψ	Electrostatic potential

CHAPTER 1

INTRODUCTION

1. Background

A wide range of chemical species ranging from small molecules to peptides are known to function as neurotransmitters and play a role in a variety of biological conditions ranging from cognition and arousal to disease and addiction [1]. While the synaptic gap between neurons is smaller (~20 nm) than current probes, neurotransmitters not bound to receptors, reuptaken or degraded diffuse into the much larger extracellular matrix of the brain. Dynamics in these neurotransmitters in live animals in response to external stimulus are usually measured by sampling the extracellular matrix with some changes in the subsecond regime. While several of these species are widely studied, neuropeptides are more difficult to study because of their low concentration (<100 pM) and lack of electrochemical sensors to detect them [1-4]. The neuropeptides neurotensin, the enkephalins, and beta-endorphin have been implicated in a variety of behaviors and diseases including feeding, pain, drug abuse, Parkinson's and schizophrenia [5-7]; moreover, current techniques are limited to quantifying these peptides at a temporal resolution of ~30 minutes [8].

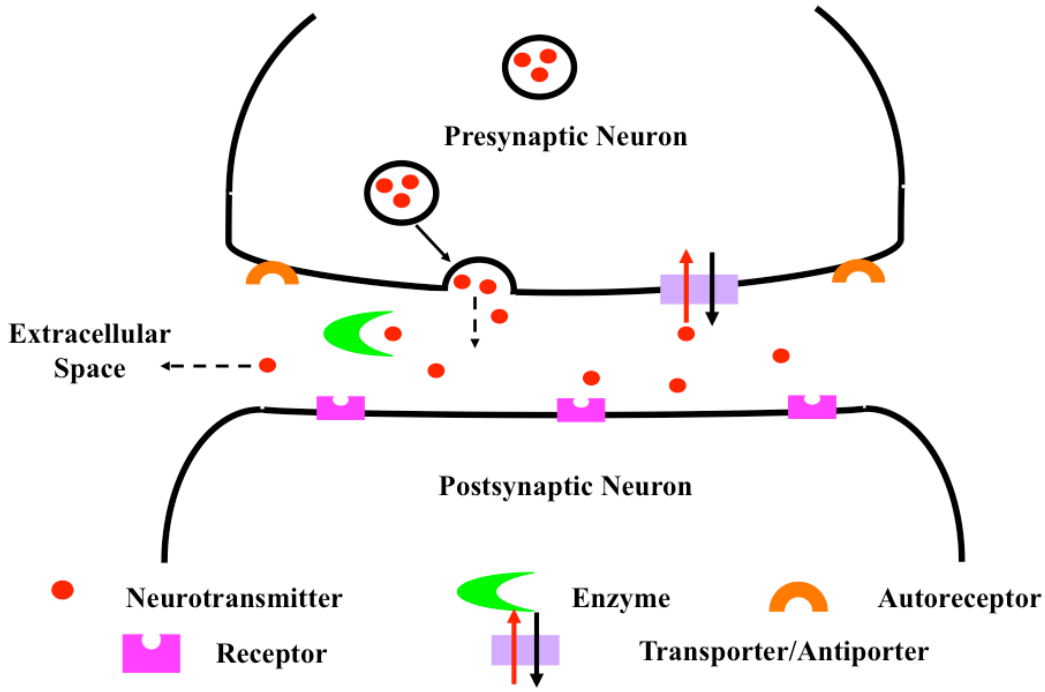

Figure 1.1. Neurotransmission across a synapse (~600 nm) via chemical transmitters released by an action potential from the pre-synaptic neuron is depicted in the scheme. Chemical neurotransmitters (red) are either uptaken by the pre- or post-synaptic neuron via transporters (purple), enzymatically degraded (green) or diffuse into the extracellular space (dashed arrow).

Quantitative analytical methods for measuring the dynamics of neuropeptides include microelectrodes and imaging techniques such as positron emission tomography. These techniques allow high temporal resolution and noninvasiveness, respectively, but with a limited range of analytes and insufficient spatial resolution for rodent studies, respectively [3, 4, 9]. Microdialysis sampling, where analytes diffuse across a hollow fiber membrane into a perfusing stream and are convectively transported to the detection system, allows quantification and is easily coupled to traditional analytical techniques such as LC-MS, HPLC and radioimmunoassay [3, 10, 11]; however, a major limitation of this method is the large sample requirements for these detection techniques.

2. Microfluidic Devices

Rapid advances in fabrication technology in the semiconductor industry has resulted in both the ubiquity of digital electronic devices throughout our lives and results in a logarithmic decrease in scale of features fabricated [12]. The application of this technology to the miniaturization of chemical instrumentation is known as microfluidics [13]. As discussed in numerous reviews, microfluidics offers several advantages over conventional analysis including, but not limited to, rapid mixing, small sample and reagent use, portability, reduction in analysis cost, and unique phenomena due to the physical forces that dominate at scales near 1 micron [14-19]. While a microfluidic platform was chosen due to its compatibility with the small sample volumes resultant from microdialysis sampling, microfabrication also allows for the integration of several of these advantages into our analytical device. Specifically, the device described herein utilizes the small scale for rapid mixing of reagents and the fluid flow is then segmented into water-in-oil droplets to preserve temporal resolution by preventing dispersion as the sample travels to analysis [19].

3. Fluorescence Polarization Immunoassay

Immunoassays are ubiquitous in biochemical analysis. In a competitive immunoassay, the antigen of interest competes with labeled antigen for antibody binding sites such that the quantity of an analyte is a function of the ratio of bound to unbound labeled antigen [20]. Since a fluorophore will only absorb if its dipole is aligned with the electric field of the light, fluorescence is polarization dependant; specifically, if a

population of fluorophore is excited with polarized light, the polarization of emitted light is determined by the amount of rotation the species undergoes. If this population of excited molecules rotates much more rapidly than the fluorescence lifetime, then the fluorescence will be isotropic; conversely, if the fluorophore is bound to another species, then its rotation will be encumbered and the fluorescence anisotropy will be larger [20, 21]. While this method of analysis is limited to analyzing a single species, advantages include the commercial availability of antibodies to bind a wide range of analytes and the modularity of the system.

While fluorescence anisotropy immunoassays have been previously demonstrated both in our lab and commercially, this technique has not been previously coupled to microfluidics. Several groups have demonstrated advantages to using segmented flow in microfluidic devices including limiting diffusion, chaotic mixing, and confined nL volumes [19]. The combination of an immunoassay and segmented flow microfluidics allows high mass sensitivity and throughput with automation and low sample requirements.

4. On-chip Preconcentration

Several methods for concentrating peptides on microfluidic devices have been demonstrated [22, 23], including solid phase extraction [24], liquid-liquid extraction [25-29], and electrokinetic stacking or trapping [24, 30-33]. Of reported techniques, only electrokinetic trapping at micro-nano-fluidic junctions can repeatedly enrich samples by factors at and greater than 10^6 on a timescale of minutes [34]. Where nanofluidic structures are technically difficult to integrate into microfluidic devices due to a greater

than 10^4 difference in feature size, a similar enrichment phenomena has been reported by using floating electrodes patterned in a microchannel, known as a bipolar electrode [35]. In this work, we broaden the application of this bipolar electrode to be compatible with highly ionic media such as is found in neurotransmitter sampling. While the Han group has reported an integrated preconcentrator and droplet generator to reduce dilution by dispersion [36], the continuous generation of droplets at volumes smaller than the concentrated band diluted the analytes by splitting them between droplets; moreover, the large droplet storage reservoir mixed the water-in-oil droplets such that all temporal resolution was lost.

5. Finite Element Method Modeling

While direct analytical measurements are preferable, several physical and chemical parameters are not measureable at the scale of microfluidic devices. Where direct numerical solutions of the equations governing pressure-driven flow, electrokinetic flow, and mass transport cannot be directly solved, a variety of commercially available software suites allow the approximation of these equations as solvable ordinary differential equations and the discretization of these systems into grids with units sequentially solved until the error between boundaries reaches an acceptably low level [37, 38]. In this work, electrokinetic and pressure driven flow were governed by the following equations (assuming continuity):

$$\rho(\partial \mathbf{V}/\partial t + (\mathbf{V}\bullet\nabla)\mathbf{V}) = -\nabla p + \mu\nabla^2\mathbf{V} + \varepsilon\kappa^2\psi\nabla\varphi$$

where the electric field was decoupled into the external field and electrostatic field resultant from the charged walls:

$$\Phi = \varphi + \psi$$

Potentials were considered to be zero when no external potential was applied to the system. Similarly, convection and diffusion were calculated by solving Fick's Law of Diffusion (at constant temperature):

$$\partial c/\partial t + (\mathbf{V}\bullet\nabla)C = D\nabla^2 C$$

where diffusion coefficients were approximated as their corresponding literature reported values.

6. Dissertation Overview

The overall goal of this dissertation is to create an integrated microfluidic device that preconcentrates continuous *in vivo* microdialysate sampling from rodent central nervous system and quantify neuropeptides therein with a fluorescent immunoassay. While microdialysis is commonly used in sampling neurotransmitter release, the components of the microfluidic device were individually designed and tested in model systems.

First, a fluorescence anisotropy competitive immunoassay for insulin secretion from Islets of Langerhans was developed and modified for compatibility with the segmented flow system to preserve temporal resolution. This assay was then used in a microfluidic device with both integrated Islet culture and chemical gradient delivery. This device was able to measure insulin secretions in a non-destructive manner from Islets stimulated by glucose.

Next, a bipolar electrode preconcentrator was developed to function with the highly conductive media used in neurotransmitter sampling. The device was optimized

in scale for the bulk flow and low abundance of neuropeptides expected in microdialysis sampling. To prevent bubble formation prevalent under the high potentials applied in this technique, a novel method of using evacuated PDMS was employed. In a model for neuropeptide preconcentration, labeled proteins were stacked into bands and sequestered into water-in-oil droplets for analysis downstream.

Finally, several microfluidic systems were analyzed by finite element method modeling to determine both ideal performance limits and non-analytically measurable properties (e.g. shear stress and diffusion of species that could not be imaged) of the devices. A microdialysis sample probe was modeled as segments in three-dimensions to determine the effects of perfusion flow rate and geometry on sample recovery; these results were compared to experimental results. Both the Islet of Langerhans perfusion chamber, used in a variety of microfluidic devices, and an adipocyte cell culture were modeled to analyze both geometric and flow rate effects on gradient delivery and shear rate. The FPIA device was modeled to determine the effective performance of the device in rapidly changing chemical gradients, mixing of reagents, and the retention of temporal resolution; additionally; biochemical secretions from individual Islet of Langerhans were modeled.

This dissertation describes a non-destructive quantitative measurement technique widely applicable to any small biomolecule with an antibody, a preconcentration system to enrich trace neuropeptides to quantifiable concentrations, and the numerical modeling of these devices. These devices illustrate that a droplet-based FPIA is a versatile analytical technique for application in miniaturized chemical and biochemical instrumentation.

References

[1] B. Kolb, I.Q. Whishaw, Fundamentals of Human Neuropsychology, Worth Publishers, New York, 2003.

[2] D.L. Robinson, A. Hermans, A.T. Seipel, R.M. Wightman, Chemical Reviews, 108 (2008) 2554.

[3] C.J. Watson, B.J. Venton, R.T. Kennedy, Analytical Chemistry, 78 (2006) 1391.

[4] B.J. Venton, R.M. Wightman, Synapse, 61 (2007) 37.

[5] R. Caceda, B. Kinkead, C.B. Nemeroff, Peptides, 27 (2006) 2385.

[6] Y. Yu, A. Jawa, W. Pan, A.J. Kastin, Peptides, 25 (2004) 2257.

[7] A. Herz, Psychopharmacology, 129 (1997) 99.

[8] K.N. Schultz, R.T. Kennedy, Annual Review of Analytical Chemistry, 1 (2008) 627.

[9] R.M. Wightman, Science, 311 (2006) 1570.

[10] M. Sandberg, S.G. Weber, Trends in Analytical Chemistry, 22 (2003) 522.

[11] J. Ruiz-Jimenez, M.D.L. de Castro, Trends in Analytical Chemistry, 25 (2006) 563.

[12] G.E. Moore, Electronics, 38 (1965).

[13] T.M. Squires, S.R. Quake, Reviews of Modern Physics, 77 (2005) 977.

[14] D.J. Beebe, G.A. Mensing, G.M. Walker, Annual Reviews of Biomedical Engineering, 4 (2002) 261.

[15] D.R. Reyes, D. Iossifidis, P.A. Auroux, A. Manz, Analytical Chemistry, 74 (2002) 2623.

[16] H.A. Stone, A.D. Stroock, A. Ajdari, Annual Review of Fluid Mechanics, 36 (2004) 381.

[17] T. Vilkner, D. Janasek, A. Manz, Analytical Chemistry, 76 (2004) 3373.

[18] J. El-Ali, P.K. Sorger, K.F. Jensen, Nature, 442 (2006) 403.

[19] H. Song, D.L. Chen, R.F. Ismagilov, Angewandte Chemie International Edition, 45 (2006) 7336.

[20] E.F. Ullman, The Immunoassay Handbook, Nature Publishing Group, London, 2001.

[21] J.R. Lakowicz, Principles of Fluorescence Spectroscopy, Springer, New York, 2006.

[22] J.G. Shackman, D. Ross, Electrophoresis, 28 (2007) 556.

[23] J. Cheng, L.J. Kricka, E.L. Sheldon, P. Wilding, in: A. Manz, H. Becker (Eds.), Microsystem Technology in Chemistry and Life Science, Springer-Verlag Berlin, Berlin, 1998, p. 215.

[24] D. Figeys, R. Aebersold, Analytical Chemistry, 70 (1998) 3721.

[25] H. Song, J.D. Tice, R.F. Ismagilov, Angewandte Chemie International Edition, 42 (2003) 768.

[26] J.R. Burns, C. Ramshaw, Lab on a Chip, 1 (2001) 10.

[27] A. Gunther, M. Jhunjhunwala, M. Thalmann, M.A. Schmidt, K.F. Jensen, Langmuir, 21 (2005) 1547.

[28] A. Gunther, K.F. Jensen, Lab on a Chip, 6 (2006) 1487.

[29] J.G. Kralj, H.R. Sahoo, K.F. Jensen, Lab on a Chip, 7 (2007) 256.

[30] H. Yang, R.-L. Chien, Journal of Chromatography A, 924 (2001) 155.

[31] S.C. Jacobson, J.M. Ramsey, Electrophoresis, 16 (1995) 481.

[32] A.T. Woolley, R.A. Mathies, Proceedings of the National Academy of Sciences, 91 (1994) 11348.

[33] J. Lichtenberg, E. Verpoorte, N.F. de Rooij, Electrophoresis, 22 (2001) 258.

[34] Y.-C. Wang, A.L. Stevens, J. Han, Analytical Chemistry, 77 (2005) 4293.

[35] R. Dhopeshwarkar, D. Hlushkou, M. Nguyen, U. Tallarek, R.M. Crooks, Journal of the American Chemical Society, 130 (2008) 10480.

[36] C.-H. Chen, A. Sarkar, Y.-A. Song, M.A. Miller, S.J. Kim, L.G. Griffith, D.A. Lauffenburger, J. Han, Journal of the American Chemical Society, 133 (2011) 10368.

[37] S.V. Ermakov, S.C. Jacobson, J.M. Ramsey, Analytical Chemistry, 70 (1998) 4494.

[38] M. Přibyl, D. Šnita, M. Kubíček, Computers and Chemical Engineering, 30 (2006) 674.

CHATPER 2

QUANTITATIVE FLUORESCENCE POLARIZATION IMMUNOASSAY ANALYSIS OF PEPTIDE SECRETIONS IN MICROFLUIDIC DEVICES

1. Introduction

Segmented flow, in which aqueous samples are partitioned within a carrier phase of immiscible fluid, has emerged as powerful way to manipulate low volume samples (10 nL and less) in microfluidic analytical systems. This approach, which may also be considered a miniaturization of "segmented flow analysis [1, 2]", creates several advantages for analytical measurement including high surface area per unit volume [3], high throughput [4], multiplexed analysis [5], discrete sample storage [6, 7], and mitigation of dispersion in temporal sampling [8, 9]. These multiphase systems commonly consist of water-in-oil droplets produced in microfluidic devices as a result of hydrodynamic focusing [10] or shear-induced droplet breakup at a geometry such as a T-junction [11, 12].

Analytes sequestered in water-in-oil droplets have previously been analyzed by a variety of methods including: off-line analysis by fluorescence microscopy [13], off-line and on-line mass spectrometry [14-17], electrophoresis [18, 19], fluorogenic enzyme assay [8], and FRET assay [4]. Fluorescence

polarization immunoassay (FPIA) is a homogenous immunoassay method that is well-suited for analysis of low volume plugs in multi-phase systems because of the relatively simple requirements for reagent addition and optical readout. Furthermore, this method can complement enzymatic and FRET methods by providing a route for detecting nearly any small molecule that can have an antibody or aptamer raised against it. Indeed, commercially available macroscale FPIA kits and systems are routinely used for quantifying drugs and hormones (e.g. the Abbott TDx system). Further, fluorescence polarization is a highly valuable method for high-throughput screening.

The principle of a FPIA is illustrated in Figure 2.1. Fluorophores excited with polarized light will emit fluorescence with higher anisotropy as molecular volume increases due to decreasing molecular rotation [20]. In FPIA, a labeled antigen and antibody are added to a sample. In the absence of unlabeled antigen (analyte), most of the labeled antigen is bound to antibody resulting in high anisotropy. As analyte concentration increases, the labeled antigen is displaced and anisotropy decreases [21].

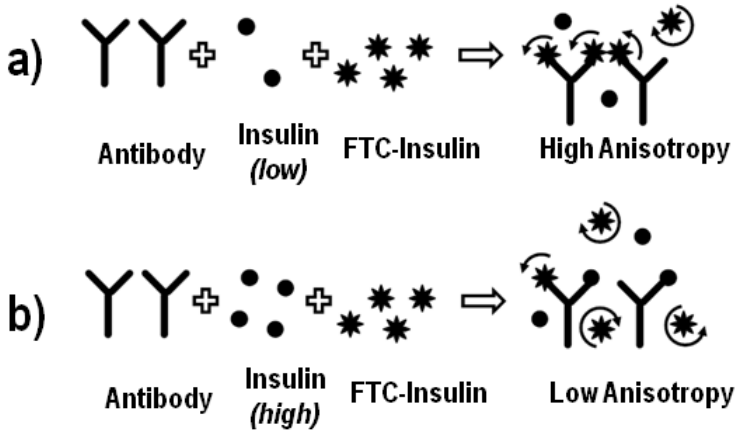

Figure 2.1. Scheme of competitive heterogeneous fluorescence polarization immunoassay in the presence of low (top) and high (bottom) antigen concentrations. Fluorescent-labeled antigens compete with unlabeled antigen from a sample matrix for binding sites on antibodies lowering the ensemble rotation of the fluorophores in an inverse relationship to antigen concentration from the sample.

In this work, we demonstrate FPIA in droplets using on-line addition of reagents to a sample stream. The system is applied to measurement of insulin release from single Islets of Langerhans perfused in culture on a microfluidic chip. Islets are micro-organs within the pancreas that contain several types of endocrine cells including insulin producing β-cells [22]. Interest in Islet secretory function is driven by the relationship between declines in insulin release and development of type-2 diabetes. Methods for monitoring insulin secretion are valuable for determining kinetics of insulin secretion during physiological manipulation of Islets and possibly for evaluating Islets to be used for Islet transplant.

Traditional methods of insulin quantification are radioimmunoassay and ELISA. These methods typically have slow feedback and are expensive to use if high temporal resolution is required because of the many samples that must analyzed. Our group has developed electrophoretic immunoassay schemes that have good temporal resolution at low cost per assay [23]. Fluorescence correlation spectroscopy in a plug format [5] has also recently been used to monitor insulin secretion from single Islets. We demonstrate that FPIA in droplets has the potential to be a simple method for monitoring insulin release with high temporal

resolution. The use of segmented flow allows maintenance of high temporal resolution for the measurement.

2. Experimental

2.1 Chemicals and Reagents

KCl, $MgCl_2$, $CaCl_2$, HF, HNO_3, $H2SO_4$, H_2O_2, NH_4OH, EDTA, NaCl, HCl, NaOH and methanol were obtained at the highest quality from Fisher Scientific. Insulin labeled with fluorescein isothiocyanate (FTC-insulin) and insulin antibody used in the immunoassay were purchased from Invitrogen and Biodesign International, respectively. Tricine, electrophoresis grade albumin from bovine serum (BSA), insulin from bovine pancreas (insulin), trichloro(1H,1H,2H,2H-perfluorooctyl)silane (FTS), anhydrous hexanes, anhydrous chloroform, fluorescein, perfluorodecalin (oil) and molecular sieve, 2A were all purchased at the highest purity from Sigma.

2.2 Solutions and Buffers

All aqueous solutions were prepared with 18 M-Ohm water (Millipore, Bedford, MA), were pH balanced with addition of 1 M NaOH, and were filtered with a 0.40 um filter. Immunoreagent buffer (IMR) consisted of 50 mM NaCl, 1 mM EDTA and 20 mM tricine, while balanced salt solution (BSS) was comprised of 125 mM NaCl, 5.9 mM KCl, 1.2 mM $MgCl_2$, 2.4 mM $CaCl_2$, 25 mM tricine. Both solutions were adjusted to pH 7.4 with dropwise addition of 1 M NaOH and 0.7 mg/mL of bovine serum albumin (BSA) was added.

2.3 Microfluidic Device Fabrication

An emulsion plot from a computer aided drafting design was printed at 50400 dpi resolution (Fineline Imaging, Colorado Springs, CO). This master design was transferred to 1.1 mm thick Borofloat® glass substrates (Telic Company, Valencia, CA) coated with 120 nm chromium and 530 nm AZ1518 photoresist (Clariant, Summerville, NJ), respectively, by exposing the substrate to 2 s of UV light (26 mW/cm2) while spatially filtered by the emulsion plot and removal of exposed photoresist and chrome with AZ915 MIF developer (Clariant, Summerville, NJ) and CEP-200 chrome etchant (Microchrome Technologies, San Jose, CA), respectively. 80 μm deep channels were wet chemically etched in 48/17/35% HF/HNO_3/H2O and verified with a Dektak 4 profilometer (Veeco Instruments Inc., Plainview, NY). Access holes to channels were drilled with 300 μm diameter diamond tipped drill bits (KYOCERA America, Inc., San Diego, CA) on a 10" drill press and substrates were bonded to Borofloat® 1.1 mm thick coverslides after sonication and cleaning in 2:1 H_2SO_4/H_2O_2 (v/v) for 10 minutes and 5:1:1 $H_2O/NH_4OH/H_2O_2$ (v/v) for 20 minutes prior to bonding substrates to coverslides between MACOR ceramic plates (Astro Met, Cincinnati, OH) in a glass kiln for 6 hours at 610 °C.

Connections to the device were made with Nanoport reservoirs (IDEX® Health & Science, Oak Harbor, WA) and 75/360 μm i.d./o.d. fused silica capillary. Capillaries used for droplet detection (outlet capillaries from the devices) were 55 cm in length with the polyimide coating burned from a 2 mm

window 50 cm from the end of the capillary that was carefully aligned to fit in the outlet access hole.

2.4 Surface Modification

All channels of devices were modified by silation chemistry [24]. Unless otherwise stated all solutions were pumped at 20 μL/min for 30 minutes. Channel and capillary walls were cleaned with 500 mM NaOH, rinsed with 18 MΩ water, activated with 1 M HCl and dried with methanol. While priming the device with anhydrous hexane, a 5 mM solution of FTS in 3:1 (v/v) hexane/chloroform was prepared. This silation solution was pumped at 10 μL/min for an hour before rinsing with anhydrous hexane and drying with methanol. Outlet capillaries, which transport droplets off-chip, were modified in a similar manner. Hydrophobic regions were removed from the perfusion channel, Islet chamber and reagent channels by pumping 500 mM NaOH through these channels while pumping methanol through the oil and droplet channel/capillaries. All devices were dried with methanol and stored in a desiccator prior to use.

2.5 Droplet Generation and Device Operation

For experiments, the device was mounted over a resistive heater strip that covered the cell chamber. Voltage was applied to the strip to maintain a temperature of 37 ^{o}C in the cell chamber. Fluid flow in the device was driven by CMA/102 (CMA Microdialysis, Sweeden) and PHD 2000 (Harvard Apparatus,

Holliston, MA) syringe pumps fitted with gas-tight syringes (Hamilton, Reno, NV). Flow through the perfusion inlets was driven at a total of 1 mL/min. Perfluordecalin was pumped at 1-2 mL/min. The oil flow rate was adjusted to generate plugs at 3-5 Hz. Chemical gradients in perfusion media over time were generated on-chip by variation of flow rates for perfusion inlet channels while maintaining a constant total perfusion flow rate of 1 μL/min. Switching of pump rates was controlled remotely by serial cable with in-house written software.

2.6 Fluorescence Anisotropy Detection

Plugs generated on-chip were pumped on-line into a capillary that was mounted in a fluorescence anisotropy detector similar to that described elsewhere [25-27]. Briefly, fluorescence was excited in the plugs within the capillary as they flowed through a focused 488 nm laser beam (Sapphire 488 30 CDRH, Coherent, Santa Clara, CA). The detection point was 50 cm downstream of the microfluidic chip. Parallel and perpendicular polarized fluorescence signal was collected at 100 Hz by in-house written LabView 8.5 virtual instrument (National Instruments, Austin, TX) with SR570 low noise current preamplifiers (Stanford Research Systems, Sunnyvale, CA). Signals were adjusted for baseline and differences in detector sensitivity (i.e., the G-factor) [20]. Droplet data points were parsed from trace for each channel and anisotropy (r) calculated by the equation:

$$r = \frac{I_{parallel} - G \times I_{perpendicular}}{I_{parallel} + 2 \times G \times I_{perpendicular}}$$

Anisotropy values were averaged for every droplet and were plotted as a function of time. For each experiment, parallel and perpendicular signals for fluorescein were measured and use to solve for the G-factor to match the literature anisotropy (r) value.

The fluorescence polarization immunoassay was optimized using a Fusion microplate reader (PerkinElmer, Waltham, MA). Insulin in BSS solution was mixed with half volume equivalents of FTC-insulin and antibody in IMR solution in microcentrifuge tubes and then transferred to a 384-well microplate for measurement assuming a 60 s incubation time.

2.7 Numerical Modeling of Sampling Single Islets with Perfusion

The performance of the perfusion chamber was numerically modeled in three dimensions using commercial finite element software, COMSOL 3.3 (COMSOL, Inc., Burlington, MA). Channel shapes were approximated as parallelogram with a height of 80 μm and top and bottom widths of 160 and 80 μm, the perfusion chamber was approximated as a 1100 μm tall cylinder with 360 μm diameter, and the Islet was approximated as a 150 μm sphere centered 70 μm from the bottom of the chamber. Viscosity and density of water were assumed to be 6.90×10^{-4} Pa s and 993 kg m^{-3}, respectively. The diffusion coefficient at 37 °C was 7.30×10^{-10} m^2 s^{-1} [28].

In all models, boundaries of inlets were defined with laminar flow profiles and fluid dynamics were solved at steady state conditions first. These solutions

were then used as parameters to solve convection and diffusion over a course of 1 min with 0.01 s time steps. The effect of the perfusion chamber on temporal resolution was modeled by defining the concentration at the inlet boundary of the mixing channel, located 500 μm upstream of the perfusion chamber, as a step change 1 s after the model began. Step changes were defined as a Heaviside function with smoothed first derivative. Islet sampling performance was modeled by integrating concentration across the outlet boundary as a function of time after a step change in concentration on the Islet surface.

2.8 Switching and Mixing Performance

On-chip mixing and the temporal response of the device were analyzed by imaging gradients in time of fluorescent dye at various points on the device. BSS and 100 nM fluorescein in BSS were pumped at a combined flow rate of 500 nL/min in the respective perfusion inlets, IMR was pumped in both immunoreagent inlets at 250 nL/min, and perfluorodecalin was pumped in the oil inlet at 1000-2000 nL/min. Mixing was monitored by line-scan analysis of images collected at the beginning of the mixing channel, end of the mixing channel and just prior to droplet formation using Igor Pro 6.0.3.1 (WaveMetrics, Inc., Lake Oswego, OR). Similarly, the temporal response to changes in pumping flow rate was determined by collecting time lapse images at the three regions of interest in the mixing experiment at 1 Hz and plotting the sum of the intensity of the 5 points centered around the maximum for each line-scan at the end of the mixing channel and immediately prior to droplet formation. Temporal responses

to these gradient changes in the capillary were compared between segmented and continuous flow, where perfluorodecalin in the oil channel was replaced with IMR, by parsing parallel fluorescent signal from droplets and plotting respective of time point data. All experiments were performed in triplicate.

2.9 Fluorescence Anisotropy Immunoassay Calibration

Prior to measuring insulin released from Islets, devices were calibrated by pumping insulin standards at 500 nL/min, 60 nM FTC-insulin at 250 nL/min and 30 nM antibody at 250 nL/min into the perfusion inlets of the device (see Figure 2.2). Oil was pumped at 1500 nL/min to generate plugs that were the passed into the detector. Signal from 50 droplets for each concentration were averaged for the calibration. Fluorescence anisotropy as a function of insulin concentration was fit as a one-site, total binding curve in Prism 5 (GraphPad Software, Inc., La Jolla, CA) for quantification.

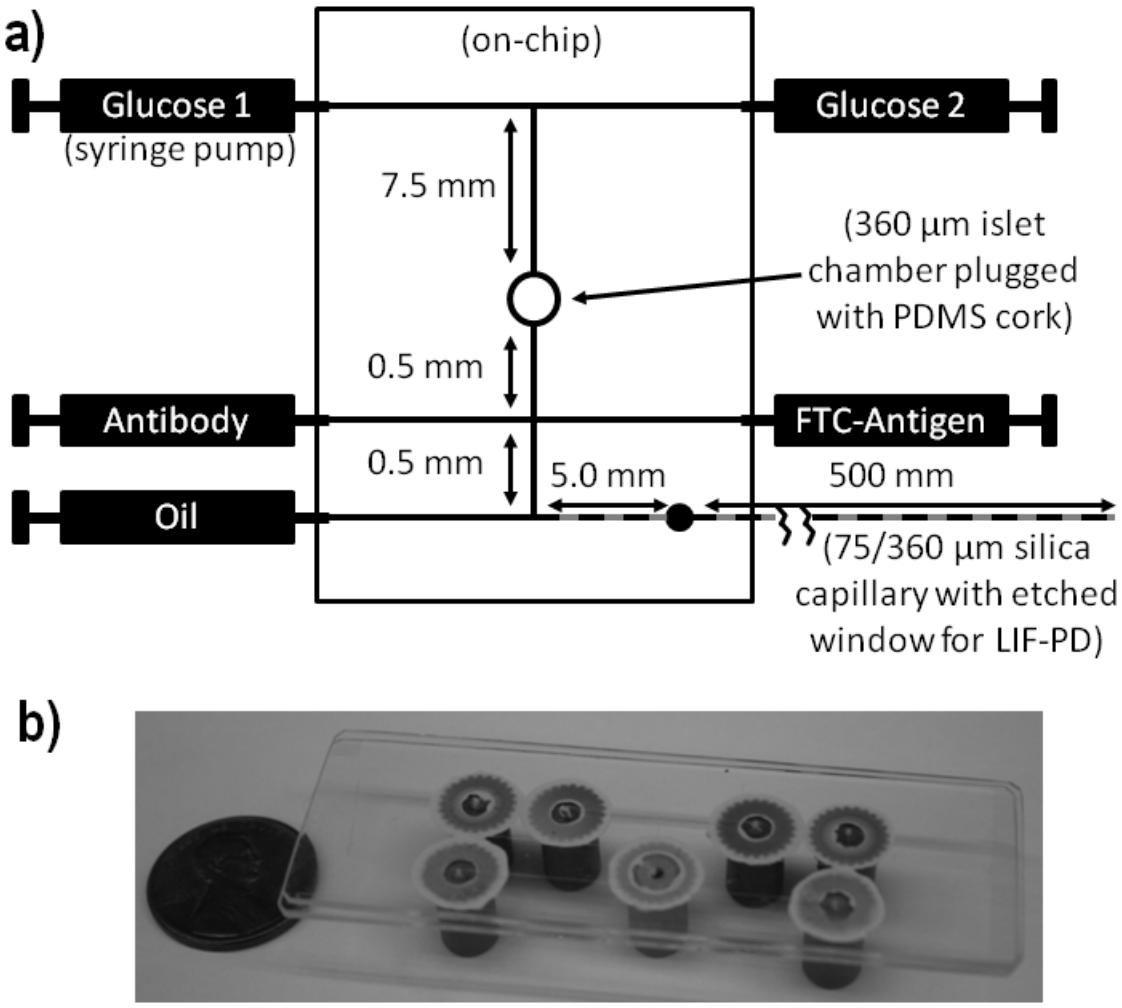

Figure 2.2. Scheme of Islet perfusion glass microchip (a) with 80 µm deep and 120 µm half width channels: droplets are formed at the interface of the aqueous (black) and oil (grey) phases and transported through hydrophobically modified channels and capillary to a laser induced fluorescence photodetection system. All flow was driven by external syringe pumps as depicted. An image of the device inverted to display channels with a cent piece for reference (b) and a cartoon of the FPIA for low and high insulin concentrations (c) are shown.

2.10 Biological Samples and Glucose Stimulated Insulin Release

Islets were isolated from male CD-1 mice as previously described [23].

Isolated Islets were incubated in RPMI 16440 media with 10% fetal bovine serum, 100 UI/mL penicillin and 100 μg/mL streptomyin for 2-5 days in an incubator maintained at 5% CO_2 and 37 ^oC before experimentation. For on-chip experiments single Islets with healthy membranes and diameters of ~150 μm were transferred to a cell culture dish with 37 ^oC BSS with 3 mM glucose added. The single Islet was then gently transferred to the Islet perfusion chamber via pipette and observed to settle on the bottom of the chamber as viewed under a stereoscope. After sealing the Islet perfusion chamber, BSS with 3 mM glucose was perfused through the Islet chamber and the plug generation was re-equilibrated.

3. Results and Discussion

3.1 Fluorescence Polarization Immunoassay Calibration and Figures of Merit

Initial experiments were directed to developing a FPIA in multiphase flow using the chip shown in Figure 2.2. In this system, a stream of insulin standard or Islet superfusate merges with streams of FTC-insulin and antibody before reaching a T-structure where aqueous plugs are formed within a carrier of oil. At plug formation rapid mixing of the reagents and sample occurs due to chaotic mixing [6] as previously modeled [29] and observed [6, 30]. Samples are then transported off the chip and through a capillary tube where they are detected in capillary using a laser-induced fluorescence polarization detector [25-27]. Parallel and perpendicular oriented fluorescence components are detected on each droplet as shown in Figure 2.3A. These signals are then converted to anisotropy

as described in the Experimental section. Increasing the concentration of insulin in the sample stream results in decreases in anisotropy as expected (see Figures 2.1 and 2.3). Flowing different concentrations through the sample channel allows calibration of the assay as shown in Figure 2.3. The sigmoidal curve response was similar to other competitive immunoassays and previously reported electrophoretic immunoassays using this antibody and FTC-insulin combination [23, 31-35].

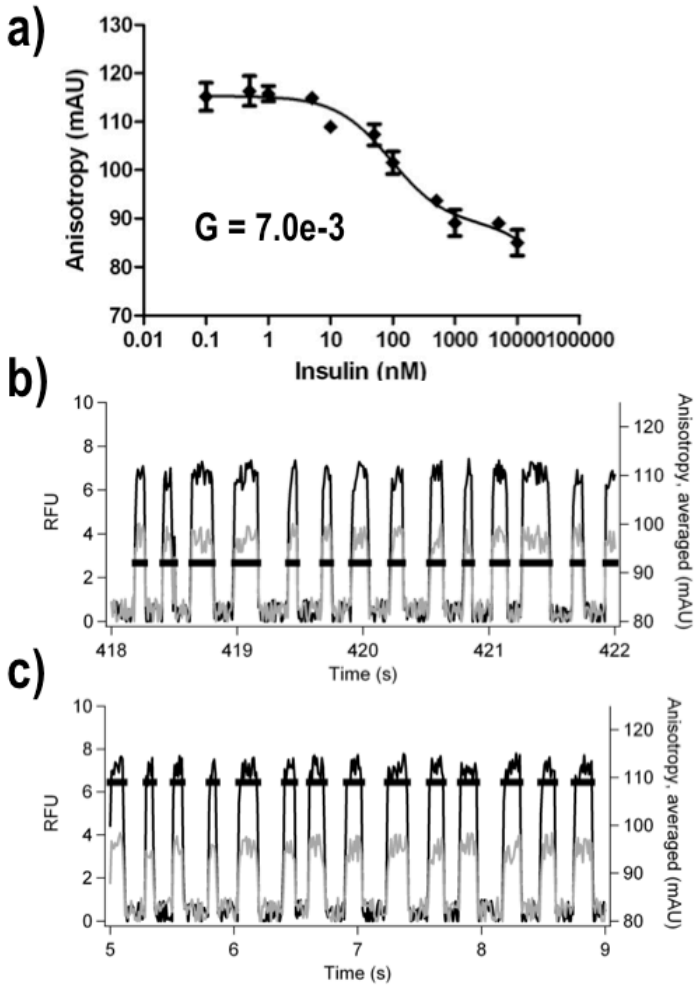

Figure 2.3. FPIA in droplet response as a function of insulin concentration with a representative calibration curve of average anisotropy from 50 droplets at various insulin concentrations with G-

factor calculated from fluorescein standards (a). Parallel (black) and perpendicular (grey) signal from plugs in capillary with calculated anisotropy (black bars) at high (1000 nM) and low (10 nM) insulin concentrations are shown in (b) and (c), respectively.

Several factors including antibody-antigen affinity, labeled-antigen fluorescent intensity and reagent concentrations determine both the limit of detection and dynamic range of a FPIA. Although antibody-antigen affinity ($K_a \sim 1\times10^9\ M^{-1}$) and fluorescent intensity are fixed for a given experiment, antigen (insulin) and immunoreagent concentrations are a function of the relative flow rates used in the perfusion system. These flow rates must be set to balance several competing performance requirements. Sample flow rate must be sufficient to rapidly wash out the Islet chamber to ensure both good temporal resolution of monitoring and adequate media flux for cell health; however, if the flow rate is too high it will overly dilute released insulin and could cause shear stress on the Islet. Additionally, the range of flow rates for sample and reagent stream and carrier fluid is constrained to regimes where droplets are reproducibly produced with sufficiently high frequency to monitor the sample and reagent stream with good temporal resolution. The flow rate also affects the concentration of reagents, which in turn influences the sensitivity range of the FPIA.

Using previous work for plug formation [8, 18], insulin competitive immunoassay [23, 31-33], and Islet release as a guide we identified the following conditions as appropriate for the monitoring insulin secretion using the FPIA:

sample flow rate = 500 nL/min, reagent flow rate = 500 nL/min (combined from equal 60 nM FTC-insulin and 30 nM antibody flow rates), and oil carrier fluid flow rate = 1000 nL/min. Using these conditions, detection limits as low as 6 nM were achieved for insulin in droplet detection. Anisotropy scaled negatively with the logarithm of insulin concentration into the μM range (see Figure 2.3). This concentration range correlates to a range of insulin secretion of ~15 to 3000 pg/min of insulin, which is within the expected range for insulin release from single Islets [36-38]. While these conditions are insufficient to measure basal insulin secretions in many experiments, recalibration at a lower flow rate lowers the detection limit and dynamic range; for example, the presence of insulin secretions below the detection limit was confirmed in each experiment by decreasing the perfusion flow rate to 250 nL/min and both immunoreagent flow rates to 125 nL/min before glucose stimulation. Improvements to the microfluidic device such as Islet chamber dead-volume, would allow more sensitive insulin measurements. Anisotropy signals for 5 nM insulin had relative standard deviations of 2.1 to 8.3% on a single chip and 13 to 19% between chips when binning signals across 2 s periods.

In the course of experiments we observed more variability in plug size, as apparent in the traces in Figure 2.3B and 2.3C, than expected. This variability was partially attributable to unexpected roughness in the surface of wet-etched channel walls. (This rough etching was eventually found to be due to poor quality in the lot of glass slides used for this work and is not expected to be a problem in future work.) A second contributor to irregular droplets was that during transfer

from the glass chip to through the irregular geometry of the drilled outlet hole-nanoport assembly minor droplet break-up and coalescence could occur. (Later work has demonstrated methods for avoiding these effects [39].) Polydispersity in droplets did not affect quantification as anisotropy was calculated for each droplet and droplets were binned. Further, droplets were created at higher frequency than the expected temporal changes in insulin.

3.2.1 Temporal Resolution

Using segmented flow allows creation of discrete samples with fixed concentrations of reagent that, except for the coalescence mentioned above, cannot mix with each other. For the application of monitoring cellular function this feature of segmented flow is advantageous in preserving temporal resolution of concentration changes even though the sample must be transported a significant distance to a detector and a sufficient incubation time is necessary for the assay. For Islet secretion measurements, temporal resolution is an important feature because insulin secretion is known to have rich dynamics including oscillations with a period of 2-5 min and possibly faster spikes with periods of 10 s [40-42].

3.2.2 Temporal Resolution (Numerical)

It was of interest to determine the temporal distortion of insulin secretion measured downstream. Unfortunately, it was experimentally difficult to make step changes of concentration within the Islet chamber, therefore the temporal

response achievable for sampling secretions from an Islet was determined by numerically modeling the three-dimensional geometry of the channels on the chip (see Figure 2.4A). Simulations showed that an instantaneous pulse of insulin released from the Islet surface was rapidly washed away from the Islet and into droplet formation channel (see Figure 2.4B). A step change from the Islet produced a 1.8 s rise time before droplet generation and transport (see Figure 2.4C). Thus, in principle this system could achieve excellent temporal resolution for Islet monitoring.

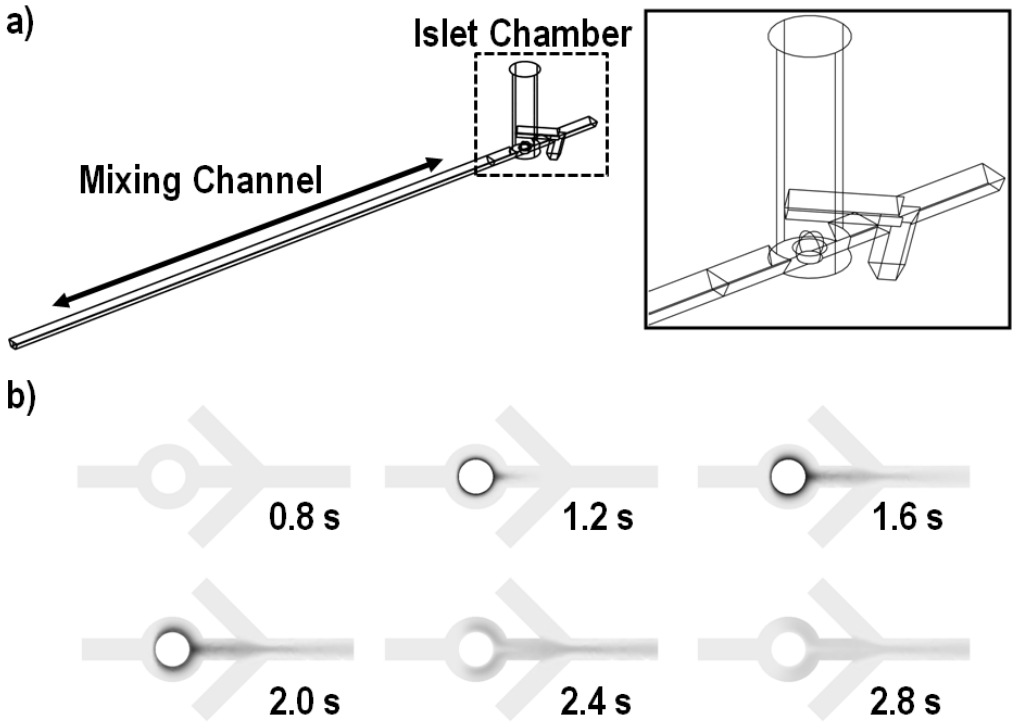

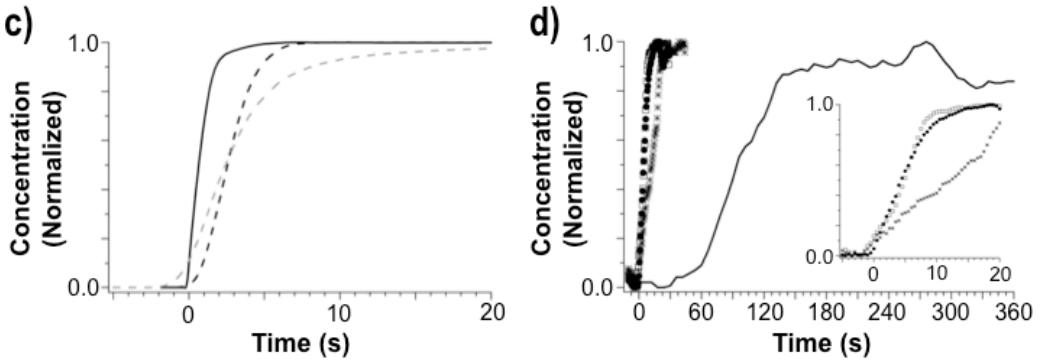

Figure 2.4. Temporal response of step changes in concentration at the perfusion inlet and Islet surface from experimental results and numerical models. The device was geometrically simplified to the regions of interest on the chip including the perfusion mixing channel, Islet chamber and reagent addition channels prior to T-junction for droplet formation (a). Time lapse images of a simulated concentration profile slice at half channel height for a 1 s pulse of insulin release from an Islet show efficient sampling in (b). Results, normalized for concentration and start frame, from the numerical model (c) and experiments with dye (d) are plotted as a function of time. In the numerical model (c), a step change at the Islet surface (solid black line) resulted in 1.8 s rise time; however, a step change in concentration at the perfusion inlet yielded a 4.8 s 10 to 90% rise time at the end of the mixing channel (dashed black line) that increased to 8.1 s after the Islet chamber and reagent addition (dashed grey line). Experimentally determined rise times from dye switching (d) yielded an 8.5 s 10 to 90% rise time at the end of the mixing channel (empty squares) that increased to 11 s after the Islet chamber and reagent addition (black circles) and to 20 s when measured in multiphase flow in capillary (stars) with an expansion in the inset. For comparison, the rise time for non-segmented flow system run under the same flow rates is shown (solid black line).

To further evaluate the temporal performance of the device, we considered how different steps in the measurement process contributed to temporal distortion using both modeling and measurements of dye fronts at different points in the

chip created by making step changes in dye at the perfusion inlet. The total temporal resolution can be considered the sum of the variances (τ^2) from pumping, pre-plug convection and diffusion on chip, and droplet formation/transport components [43, 44]. Results from numerical models predicted that a step change in concentration made at the perfusion mixing channel inlet broadens to 4.8 s (10 to 90% rise time) before reaching the Islet chamber (Figure 2.4C, dashed black line). This rise time increased to 8.1 s after the Islet chamber and reagent addition channels (Figure 2.4C, dashed grey line). These results suggest a 6.5 s of broadening prior to droplet formation and transport into the capillary based on summing the squares of the temporal contributions (see Figure 2.4C).

To confirm the validity of numerically modeled broadening, broadening of step changes in fluorophore pumped through the system were measured and compared to the model. In general good agreement was found. Experimental data from imaging showed a 7.0 s contribution (6.5 s from numerical modeling) from the increase in rise time after the Islet chamber and reagent addition (see Figure 2.4D). As a sum of squares this 7.0 s increase corresponds to a 2.5 s increase from 8.5 to 11 s of the total rise time of the analytical system. However, the system's response time increases to 20 s when measured in droplets at the detection window of the capillary. The post-plug increase in response time is caused by droplet breakup and fusion at the large, rough drilled access hole and capillary connection. Therefore, imperfections in droplet manipulation ultimately limited the temporal performance of this device.

Nevertheless, it is apparent that plug flow allowed the creation of discrete samples with fixed concentrations of reagent that cannot mix with each other; specifically, this temporal quantization of plug flow is advantageous in preserving temporal resolution for monitoring cellular function via secretory species concentration dynamics even though the sample must be transported a significant distance to a detector and a sufficient incubation time is necessary for the assay. As a demonstration of this effect, if no droplet formation is used, the broadening is about 90 s (see Figure 2.4D, solid black line).

3.3 Monitoring Islet Function

To demonstrate the use of the system for monitoring cellular function, we exposed Islets maintained in the sample chamber to step increases in glucose and monitored the insulin content of resulting plugs. Traces from several such experiments are illustrated in Figure 2.5. Islets exhibited a characteristic burst of insulin followed by elevated secretions over basal levels when exposed to increased glucose [45, 46]. In some experiments, basal concentrations were not detectable at the flow rates used. Therefore, to determine basal concentration we slowed the flow rates to half, thus achieving higher concentrations in the sample. From these measurements, average peak insulin secretions were 124 ± 19 pg/min (n = 7). Basal insulin levels were near or below the detection limit such that they were not quantified; however, the presence of insulin the perfusate was confirmed by lowering the flow rate, illustrating the trade off between sensitivity and temporal resolution. The Islets also displayed a variety of insulin secretion

dynamics that have been previously observed. These include an initial burst phase of insulin release (Figure 2.5), slow oscillations with period of 2-5 min (Figure 2.5D) and more rapid fluctuations with period of ~ 20 s (Figure 2.5C). Such rapid fluctuations are expected but have been difficult to measure by other methods.

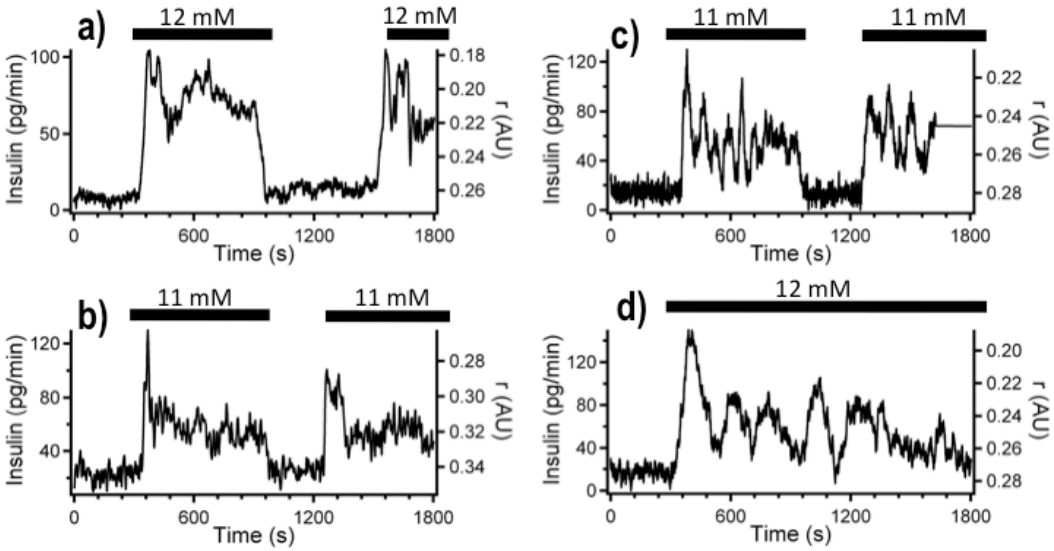

Figure 2.5. Sample traces of insulin secretion measured by FPIA in segmented flow from 4 individual Islets treated with step changes in glucose concentration (a-d).

The automated perfusion system used here allowed cycling between high and low glucose concentrations as well (see Figure 2.5A, B, C). These results show a decreased intensity of peak insulin bursts on the second stimulation. This decreased release is possibly due depletion of insulin secretory granules near beta-cell membranes by previous stimulated release [46].

Previously reported microfluidic platforms for Islet monitoring have achieved detection limits as low as 0.8 nM [33] or have used segmented flow

sampling for temporal resolution limited only by flushing the sample chamber [5]. These systems all required comparatively expensive imaging systems (microscope with camera compared to a single point detector) and were constrained in flexibility of glucose (or other chemical) concentration changes. Easley demonstrated a segmented flow system with indirect measurements of insulin secretion with dyes [47] (e.g. Fluo-4) that can be realized with a single point detector but assume a 2:6 Zn^{2+}:insulin secretion ratio; however, changes the chemical gradient supplied to the Islet caused interruptions in quantitative measurements.

4. Conclusions

Although FPIA has been demonstrated on a continuous flow microfluidic device[48], this work demonstrates that FPIA can be performed in a plug-flow system by mixing immunoassay reagents on-line with sample prior to plug formation and then monitoring the anisotropy of plugs within the tube. Rapid mixing in droplets eliminated the need for complex fabrication of mixing channels and preserved temporal resolution from sampling to quantification. This assay adds the types of assays that can be performed in plugs. The assay was applied to monitoring insulin from single Islets at high temporal resolution; however, as FPIA and other fluorescence polarization methods are commonly used for measuring drugs, hormones, and small molecule-protein interactions, this approach may prove useful when low volume and high-throughput is required such as clinical assays or high-throughput screening.

While several segmented flow devices that improve temporal resolution over continuous flow devices have been recently reported, we demonstrate a versatile analytical technique for measuring a range of pharmacologically relevant compounds with a simple detection method. This microfluidic device both improved temporal resolution by generating gradients near to the biological sample and by segmenting flow shortly downstream from the biological sample. This method allowed fast pulsatile insulin release from Islets to be measured. Numerical and analytical results suggest further improvements in temporal resolution are limited by the pumps and chip to capillary connections used in this work. Future experiments with continuous multiphase flow FPIA can also be scaled to samples accessible with microfluidics (from single cell to tissue), multiplexed with contrasting dyes or multiple channels, or remotely sampled by storing water in oil droplets in a cartridge prior to analysis.

References

[1] J. Ruzicka, E.H. Hansen, Analytica Chimica Acta, 78 (1975) 145.
[2] L.T.J. Skeggs, American Journal of Clinincal Pathology, 28 (1957) 311.
[3] M. Nakano, J. Komatsu, S.-i. Matsuura, K. Takashima, S. Katsura, A. Mizuno, Journal of Biotechnology, 102 (2003) 117.
[4] M. Srisa-Art, E.C. Dyson, A.J. deMello, J.B. Edel, Analytical Chemistry, 80 (2008) 7063.
[5] D. Chen, W. Du, Y. Liu, W. Liu, A. Kuznetsov, F.E. Mendez, L.H. Philipson, R.F. Ismagilov, Proceedings of the National Academy of Science, 105 (2008) 16843.
[6] H. Song, M.R. Bringer, J.D. Tice, C.J. Gerdts, R.F. Ismagilov, Applied Physics Letters, 83 (2003) 4664.
[7] H. Song, J.D. Tice, R.F. Ismagilov, Angewandte Chemie International Edition, 42 (2003) 768.
[8] M. Wang, G.T. Roman, K. Schultz, C. Jennings, R.T. Kennedy, Analytical Chemistry, 80 (2008) 5607.
[9] H. Song, R.F. Ismagilov, Journal of the American Chemical Society, 125 (2003) 14613.
[10] S.L. Anna, N. Bontoux, H.A. Stone, Applied Physics Letters, 82 (2003) 364.
[11] T. Thorsen, R.W. Roberts, F.H. Arnold, S.R. Quake, Physics Review Letters, 86 (2001) 4163.
[12] P. Garstecki, M.J. Fuerstman, H.A. Stone, G.M. Whitesides, Lab on a Chip, 6 (2006) 437.
[13] V. Linder, S.K. Sia, G.M. Whitesides, Analytical Chemistry, 77 (2005) 64.
[14] S. Ekstrom, D. Ericsson, P. Onnerfjord, M. Bengtsson, J. Nilsson, G. Marko-Varga, T. Laurell, Analytical Chemistry, 73 (2001) 214.
[15] A.R. Wheeler, H. Moon, C.-J.â.œ. Kim, J.A. Loo, R.L. Garrell, Analytical Chemistry, 76 (2004) 4833.
[16] L.M. Fidalgo, C. Abell, W.T.S. Huck, Lab on a Chip, 7 (2007) 984.
[17] J. Pei, Q. Li, M.S. Lee, G.A. Valaskovic, R.T. Kennedy, Analytical Chemistry, 81 (2009) 6558.
[18] G.T. Roman, M. Wang, K.N. Shultz, C. Jennings, R.T. Kennedy, Analytical Chemistry, 80 (2008) 8231.
[19] J.S. Edgar, C.P. Pabbati, R.M. Lorenz, M. He, G.S. Fiorini, D.T. Chiu, Analytical Chemistry, 78 (2006) 6948.
[20] J.R. Lakowicz, Principles of Fluorescence Spectroscopy, Spinger, New York, 2006.
[21] W.B. Dandliker, R.J. Kelly, J. Dandliker, J. Farquhar, J. Levin, Immunochemistry, 10 (1973) 219.

[22] A. Nadal, I. Quesada, B. Soria, Journal of Physiology Online, 517 (1999) 85.
[23] J.F. Dishinger, R.T. Kennedy, Analytical Chemistry, 79 (2007) 947.
[24] B. Zhao, J.S. Moore, D.J. Beebe, Science, 291 (2001) 1023.
[25] P. Yang, R.J. Whelan, Y. Mao, A.W.M. Lee, C. Carter-Su, R.T. Kennedy, Analytical Chemistry, 79 (2007) 1690.
[26] P. Yang, R.J. Whelan, E.E. Jameson, J.H. Kurzer, L.S. Argetsinger, C. Carter-Su, A. Kabir, A. Malik, R.T. Kennedy, Analytical Chemistry, 77 (2005) 2482.
[27] R.J. Whelan, R.K. Sunahara, R.R. Neubig, R.T. Kennedy, Analytical Chemistry, 76 (2004) 7380.
[28] G.D. Fasman, CRC Handbook of Biochemistry and Molecular Biology, Chapman & Hall/CRC, Boca Raton, FL, 1976.
[29] K. Handique, M.A. Burns, Journal of Micromechanics and Microengineering, (2001) 548.
[30] M. Srisa-Art, A.J. deMello, J.B. Edel, Physics Review Letters, 101 (2008) 014502.
[31] L. Tao, R.T. Kennedy, Electrophoresis, 18 (1997) 112.
[32] M.G. Roper, J.G. Shackman, G.M. Dahlgren, R.T. Kennedy, Analytical Chemistry, 75 (2003) 4711.
[33] J.G. Shackman, G.M. Dahlgren, J.L. Peters, R.T. Kennedy, Lab on a Chip, 5 (2005) 56.
[34] J. Taylor, G. Picelli, D.J. Harrison, Electrophoresis, 22 (2001) 3699.
[35] M. Jolley, S. Stroupe, C. Wang, H. Panas, C. Keegan, R. Schmidt, K. Schwenzer, Clinical Chemistry, 27 (1981) 1190.
[36] R.N. Kulkarni, International Journal of Biochemistry and Cellular Biology, 36 (2004) 365.
[37] R.A. Ritzel, J.D. Veldhuis, P.C. Butler, Journal of Clinical Endocrinology and Metabolomics, 88 (2003) 742.
[38] J. Westerlund, P. Bergsten, Diabetes, 50 (2001) 1785.
[39] J. Pei, J. Nie, R.T. Kennedy, Analytical Chemistry, 82 (2010) 9261.
[40] P. Rorsman, E. Renstrom, Diabetologia, 46 (2003) 1029.
[41] H. Kang, J. Jo, H.J. Kim, M.Y. Choi, S.W. Rhee, D.S. Koh, Physics Review E, 72 (2005) 051905.
[42] P.E. MacDonald, P. Rorsman, Public Library of Science Biology, 4 (2006) e49.
[43] W. Feller, An introduction to probability theory and its applications, Wiley, New York, 1967.
[44] J.C. Giddings, Unified Separation Science, Wiley, New York, 1991.
[45] R.T. Kennedy, L.M. Kauri, G.M. Dahlgren, S.-K. Jung, Diabetes, 51 (2002) S152.
[46] C.J. Hedeskov, Physiology Reviews, 60 (1980) 442.
[47] C.J. Easley, J.V. Rocheleau, W.S. Head, D.W. Piston, Analytical Chemistry, 81 (2009) 9086.
[48] T. Tachi, N. Kaji, M. Tokeshi, Y. Baba, Lab on a Chip, 9 (2009) 966.

CHAPTER 3

MICROFLUIDIC BIPOLAR ELECTRODE PRE-CONCENTRATION IN HIGHLY CONDUCTIVE MEDIA

1. Introduction

The quantification of neurotransmitters *in vivo* enables the direct study of the biochemical pathways in both normally functioning and diseased states of the brain [1]. While numerous neurotransmitters are known to range from small molecules like nitrous oxides to large peptides like the endorphins, the low concentration of several of these biochemical species in the highly complex matrix of the central nervous system have frustrated efforts to directly study these pathways. To reach levels of mass detection, either large a sample must be collected (which limits temporal resolution) or the samples concentrated prior to analysis [2, 3]. Several methods for pre-concentration have been reported, including solid phase extraction (SPE) [4-6], isoelectric focusing (IEF) [7, 8], temperature gradient focusing (TGF) [9, 10] and electric field gradient focusing (EFGF) [11-13]. Of preconcentration methods that can be continuously reused in a microfluidic device, the highest reported rate of enrichment reported is 10^8-fold in an hour from an EFGF method known as ion concentration polarization (ICP) [14].

ICP, first observed by Rubinstein in desalination experiments with membranes, is a phenomenon in which bulk charge is primarily carried by either cations or anions at a greater flux than those ions are replaced such that localized region depleted of ions results [15-17]. This depleted region will have several implications for the electrochemical circuit: first, the electric field will have a larger gradient in the regions of concentrated ions that accumulate on either side of the depletion region; and, second, as the depletion region lowers the ionic strength of the solution sufficiently, the double layer formed by counterions at the charged surfaces of the walls will overlap inducing a permiselective region which only facilitates the transport of ions of the same charge as the double layer [18-24].

Two methods to engender ICP include the junction of a micro- and nano-channel under an electrical potential of sufficient strength to cause the double layers to overlap or by patterning a conductive material that is free to float in a channel of a microfluidic device. This bipolar electrode (BPE) offers an alternate, lower resistance path for current that reduces the electric field near the electrode; additionally, the ends of the electrode allow water-splitting and other gas generating reactions to occur which will break the electrical circuit once comparable in size to the channel [8, 25-39]. To overcome this limitation, buffers are carefully chosen to reduce gas generation or that require lower potentials such as low ionic strength sample matrices. In this chapter we will describe a microfluidic device that repeatedly pre-concentrates negatively charged peptides in highly ionic solution without bubble formation. While a variety of quantification methods are compatible with this device, water-in-oil droplets were generated to store the

pre-concentrated peptides for compatibility with the quantification method described in the previous chapter.

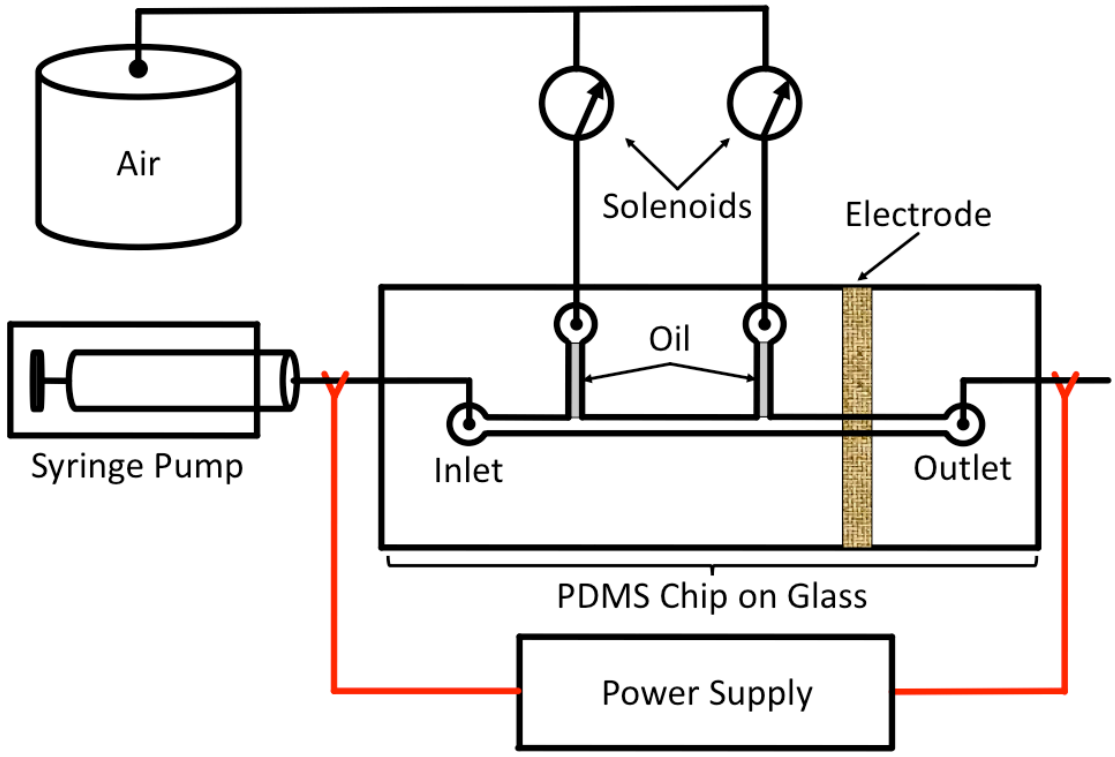

Figure 3.1. Scheme of bipolar electrode preconcentrator device where 100 µm channels in PMDS are bonded to a glass substrate with a Ti/Au electrode. Aqueous sample driven by syringe pump into the main channel and oil driven (on demand) by pressurized air into two perpendicular channels were connected to the inlet reservoirs with 90-degree syringe tips. Electrical potentials were applied from a DC source to the syringe tips at the aqueous inlet and outlet.

2. Materials and Methods

2.1 Chemicals and Solutions

Fluorescein, sodium chloride, potassium chloride, magnesium sulfate, calcium chloride and phosphoric acid (both potassium and disodium salts) were purchased at the

highest purity from Sigma-Aldrich (St. Louis, MO). Phosphate buffered saline (PBS: 137 mM NaCl, 2.7 mM KCl, 10 mM Na_2HPO_4, 1.76 mM KH_2PO_4, pH 7.4) and artifical cerebral spinal fluid (aCSF: 145 mM NaCl, 2.68 mM KCl, 1.01 mM $MgSO_4$, 1.22 mM $CaCl_2$, 1.55 mM Na_2HPO_4, 0.45 Mm NaH_2PO_4, pH 7.4) solutions were prepared by dilution of reagents in 18 MΩ (MilliQ, Millipore, Bedford, MA) and pH adjusted with HCl. Insulin, human recombinant from *E Coli*, fluorescent conjugate (Invitrogen, Carlsbad, CA) was diluted in PBS to 1.633 mM and stored protected from light at -5 C until use in experiments.

2.2 Device Fabrication

Polydimethylsiloxane (PMDS) fluidic layers were produced using normal lithographic techniques [40]; specifically, SU-8 2075 (Microchem, Newton, MA) was spun to 100 μm on mechanical grade 150 mm Si wafers and patterned by exposure to collimated UV light masked through a 56000 dpi transparency film (Fineline Imaging, Colorado Springs, CO) prior to development as per the manufacturers instructions. Well-mixed and degassed PDMS was poured over molds and cured at 100 °C overnight to cure. After punching reservoirs through the PMDS layer with a biopsy punch, PMDS layers were plasma bonded (Electrotechnic, Chicago, IL) to glass slides with liftoff patterned 1 mm wide 50/250 Å Ti/Au electrodes.

2.3 Fluidic Control

Aqueous solutions were driven by syringe pump (CMA Microdialysis, Solna, Sweeden) connected via Teflon® tubing connected to 90-degree syringe tips inserted into

inlet reservoirs in the PDMS layer of devices; similarly, oil channels were driven by computer controlled pulsed air in Teflon® tubing connected to 90-degree syringe tips inserted to oil inlet reservoirs in the PDMS layer. While aqueous solutions were continuously delivered at volumetric flow rates from 0.2 to 10 μL/min, oil solutions were only driven on-demand as controlled by an in-house written VI (LabView 8.5, National Instruments, Austin, TX).

2.4 Electrical Control

Electrical fields were applied by adjusting M10-S500 power supplies (American Power Design, Windham, NH) to desired voltages with an HHM 93 digital multimeter (Omega, Stamford, CT) and then clipping the power supply anode and cathode at the 90-degree syringe tips inserted into the inlet and outlet reservoirs, respectively. Potentials above 600 V were achieved by connecting power supplies in series.

2.5 Experimental and Image Analysis

Concentration experiments were imaged on a SZH10 stereoscope (Olympus America, Center Valley, PA) with 480 nm band-pass filtered BH2-RFL-T3 Hg arc lamp (Olympus America, Center Valley, PA) excitation. Images for quantification were collected with a Andor Newton ECCD camera and calibrated by average photon counts per pixel as measured with serial dilutions of fluorescein standards (1 mM, 1 μM, 1 nM, 1 pM, and 1 fM, specifically). Image analysis was performed in ImageJ (NIH, Bethesda, MA).

3. Results and Discussion

3.1 Ion Concentration Polarization via a Floating Bipolar Electrode

To maintain an open circuit by preventing bubble formation the flux of gas diffusing out of the channel must be greater than the formation of gasses in the channel. While the flux of gases out of the channel is increased by the use of gas permeable substrates such as polydimethylsiloxane (PDMS), vacuuming PDMS increases this flux and is known to prevent bubble formation [41]. Specifically, we observed that storing the devices in vacuum to evacuate the gasses from the PDMS allowed the application potentials as high as 2 kV in media of >150 mM ionic strength in excess of 1 hour without observable bubble formation.

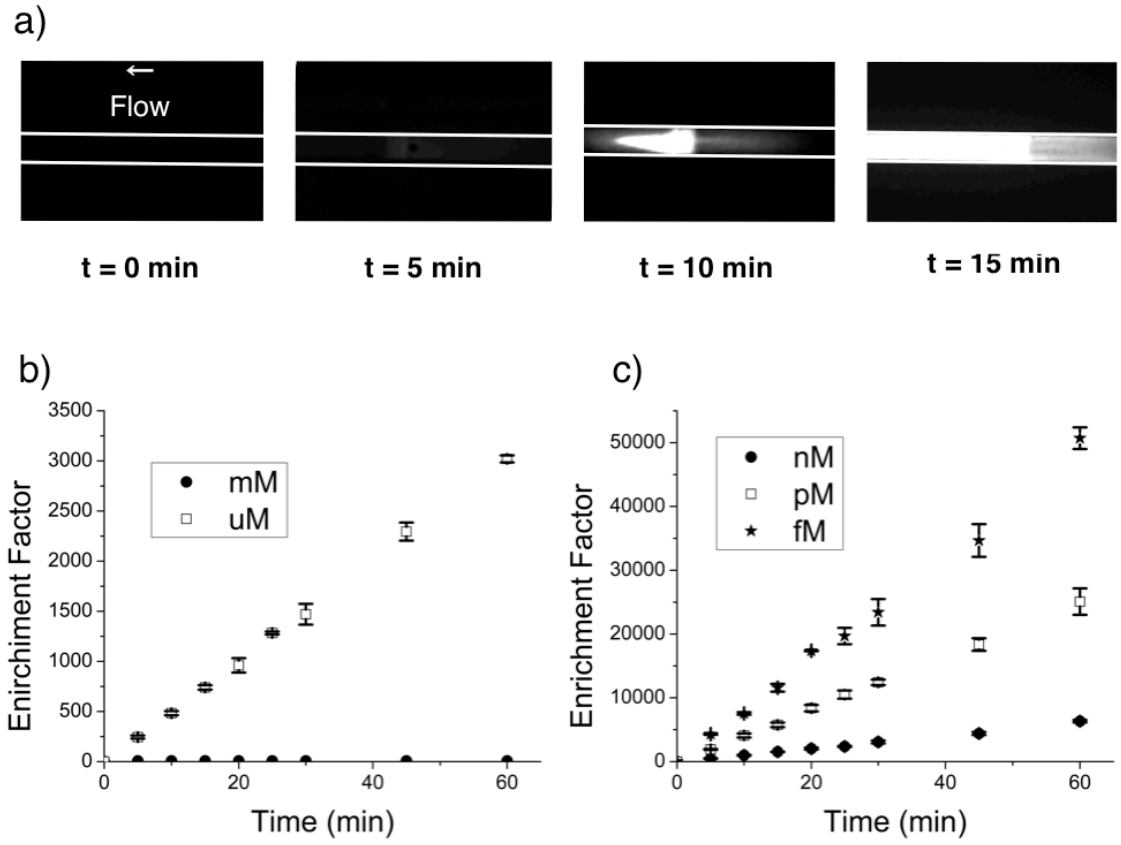

Figure 3.2. Time-lapse images (a) of ICP effect of 100 nM FITC-insulin in aCSF at 600 V in a 100 μm wide PDMS channel. Plots of enrichment factor of 1 mM and 1 μM (b) and of 1 nM, 1 pM and 1 fM (c) FTC-insulin in PBS as a function of time under an electric field of 250 V.

3.2 Media, flow rate, and voltage on enrichment

Several parameters including media, bulk flow rate, and voltage were considered in optimizing devices for concentration of neuropeptides sampled from microdialysis. First, while the high ionic strength sample media of aCSF limits the rate of enrichment due to the high conductivity in the channel [26, 29, 32], dilution of the sample both increased the analysis time and yielded lower final concentrations of dyes for a given enrichment period. For example, a 1 nM FITC-insulin in aCSF was enriched to 1 mM with 30 min, where the same sample diluted by a factor of 10 required over 1 hour to

reach the same fluorescent intensity. Similar results were observed with dilutions of PBS, such that undiluted samples were used.

Second, the bulk flow rate of sample introduction was tested with a range of microdialysis flow rates used in similar in vivo experiments; specifically, in the range of 0.2-10 μL/min. While higher flow rates are known to have lower relative recovery due to the shorter exposure to the diffusive region of the probe, the total flux of sampled species increases with flow rate as the larger chemical gradient into the probe linearly increases the rate of diffusion. Experimental limitations of syringe pump speeds and tissue damage generally limit flow rates to <10 μL/min. Both the stability of the location of the concentrated band generated and rate of enrichment increased linearly with increasing flow rate such that 10 μL/min was found to be the optimal bulk flow rate.

Third, voltages from zero to 1200 V were tested by quantification of enrichment of a 10 nM FTC-insulin after 10 minutes of applied voltage (see Figure 3.3). Where no enrichment was observed in the absence of an electric field, the rate of enrichment increases linearly with respect to electric potential at values below 400 V. Rates of enrichment did not significantly vary at voltages above 400 V suggesting that enrichment was limited either by the rate of redox reactions at the BPE or delivery of sample by bulk flow.

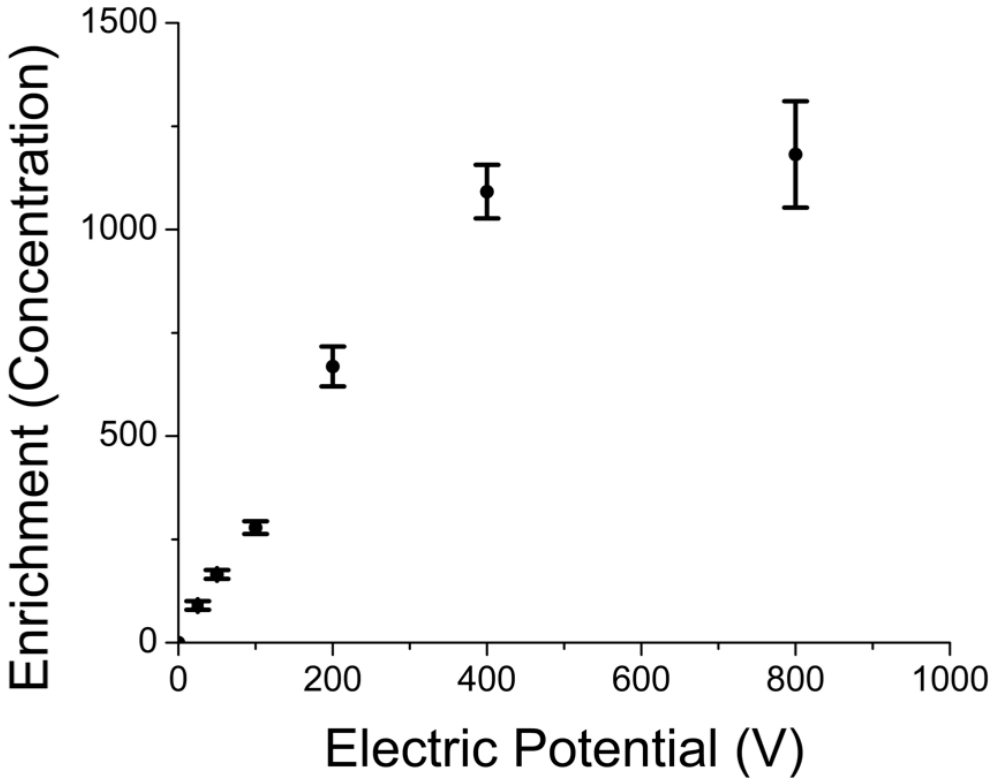

Figure 3.3. Enrichment factor of 100 nM FITC insulin in PBS as a function of voltage applied after 10 minutes.

3.3 Rate of Enrichment

Several factors including but not limited to the ionic strength of the solution, choice of buffer, electrical potential applied and initial concentration effect the rate of enrichment of charge species in the BPE concentrators studied. While the application to neuropeptide pre-concentration limits the sample matrix to high ionic strength and sub nM concentrations of analytes, a 250 V potential was used test the feasibility of multiplex pre-concentrator with low power consumption. As previously reported, highly concentration solutions appeared to enrich more slowly than analytes initially present in trace amounts (see Figure 3.2); however, as 1 mM fluorescein was near the solubility

limit in PBS and was calibrated to within an order of magnitude of maximum signal from the detector, saturation occurred within 5 minutes such that the rate could not be quantitatively measured.

Approximation of enrichment as a function of time yielded fits with coefficients of determination of 0.995 or greater; specifically, rates were calculated by applying a Gaussian linear regression of extrapolated concentrations as a function of time with the electrical circuit active. Under a 250 V potential, devices enriched 1 μM FITC-insulin at a rate of 3041 ± 29-fold/s. This rate increased to 6218 ± 132-fold/s for 1 nM and increased to 25039 ± 246-fold/s for 1 pM FITC-insulin. Following this trend of more rapid enrichment at lower initial concentrations, 1 fM FITC-insulin was enriched at a rate of 49300 ± 1330-fold/s. While previous reports have suggested the initial concentration of analyte effects enrichment rates due to changes in the ionic strength of the media, the low relative (> 1%) contribution to ionic strength of the sample matrix illustrate the initial ionic strength is not the main contribution to this phenomena.

3.4 Droplet Generation and Capture of Band

To optimize the capture of bands in water-in-oil plugs, the location of the band after 1 hour of concentration was observed to occur within 1.7 to 2.5 mm (varied between devices) upstream of the cathode end of the BPE. The fluidic layers of devices were bonded such that oil channels, perpendicular channels to the concentration channel, would be located on either side of this concentration region. Droplets were generated at a variety of sizes as a function of spacing the oil inlet channels during fabrication such that 5, 10 and 20 nL volume droplet devices were tested. Droplets were produced as 5.62 ±

0.65 nL, 10.32 ± 0.48 nL and 20.57 ± 2.60 nL droplets as approximated as rectangular plugs from imaging.

Sequestration of enriched bands in water-in-oil droplets was manually triggered with relative reproducibly in 5 nL and larger droplets (see Figure 3.4). To ensure the highest enrichment the droplet must be large enough to encapsulate the entire band while excess volume of the droplet beyond this size will linearly dilute the enriched region. In the case of 5 nL droplets, an efficiency of 58.4 % capture of the concentrated band lowered the effective enrichment to 5953-fold. While 10 nL droplets increased in efficiency of droplet capture to 94.7 % and 20 nL droplets retained 98.7 % of the enriched band total fluorescence after droplet generation, the 10 nL droplet resulted in a 5022-fold enrichment over the 3021-fold in the more dilute 20 nL droplet. Droplet volumes with less than twice the length of the enriched band were experimentally difficult to manually confine into water-in-oil plugs. Experimentally, the use of smaller droplets resulted in the most concentrated plugs of pre-concentrated sample despite high loss (>25%) of enriched ions due to convective flow during droplet generation.

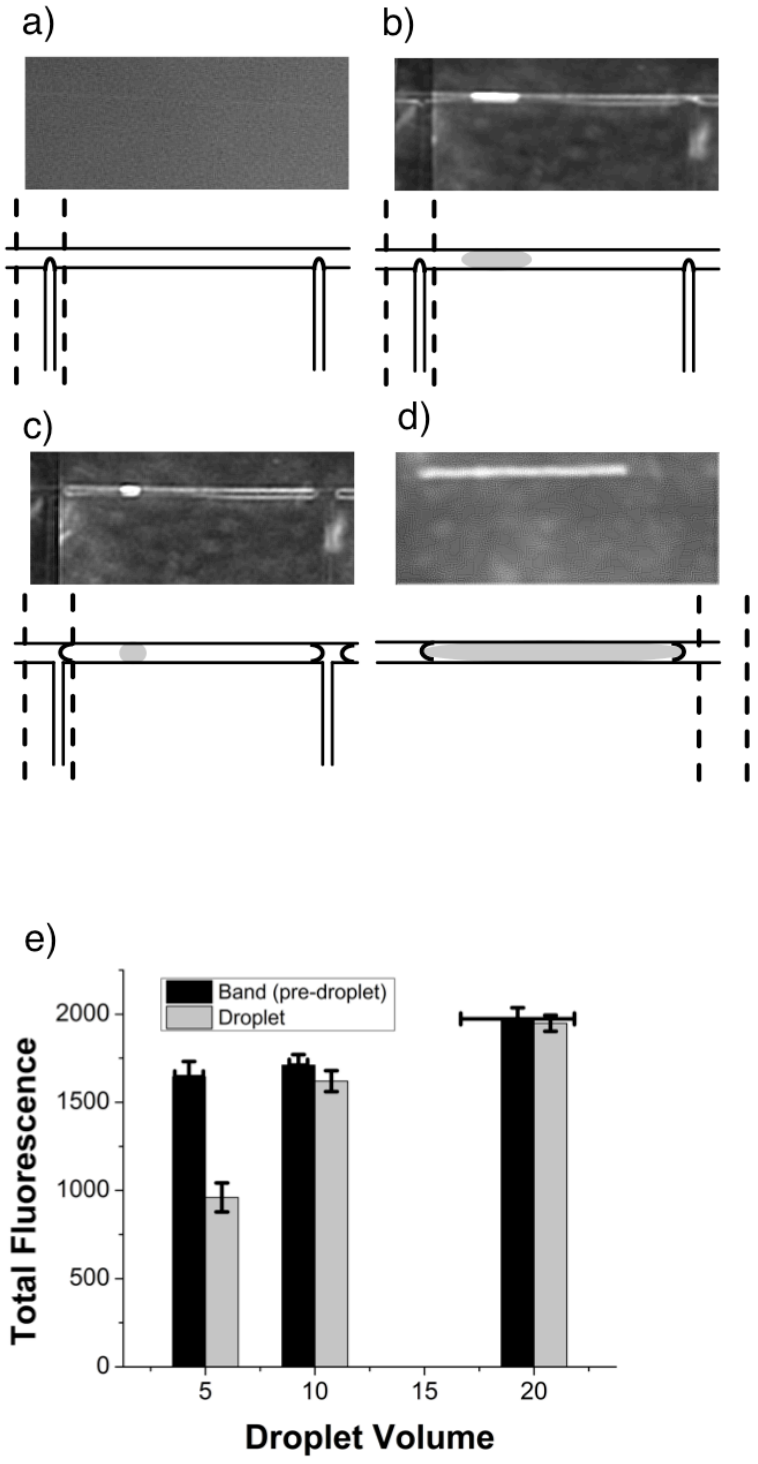

Figure 3.4. Time-lapse images with bright-field and fluorescent illumination of enriched band immediately before (b) and after droplet generation (c) show compression of the band during droplet generation. Contrast enhanced fluorescent images of the initial sample solution (a) and droplet with captured enriched

band (d) for 1 nM FITC-insulin in PBS after 30 min enrichment at 250 V illustrates the relative pre-concentration of samples. In the bar graph (e), the total fluorescence of the enriched region (dark) before and after droplet generation and transport to the exit reservoir (grey) shows the relative efficiency of droplet capture as a function of volume.

4. Conclusions

In this chapter we present the first microfluidic pre-concentrator with segmented flow (water-in-oil droplet) sequestration. Where this droplet storage is directly compatible with the fluorescence polarization immunoassay quantification discussed in the previous chapter, this device enables the quantification of any biochemical species with commercially available antibodies. Droplet sequestration of concentrated bands of analytes additionally allows storage for further analysis.

While improvements in future generations of devices allow room for improvements in capture efficiency by changing the geometry, the device reported achieved enrichment of a negatively charged protein in highly ionic media on the order of 50000 in 1 hour with capture efficiency as high as 99%.

References

[1] B. Kolb, I.Q. Whishaw, Fundamentals of Human Neuropsychology, Worth Publishers, New York, 2003.

[2] D.L. Robinson, A. Hermans, A.T. Seipel, R.M. Wightman, Chemical Reviews, 108 (2008) 2554.

[3] C.J. Watson, B.J. Venton, R.T. Kennedy, Analytical Chemistry, 78 (2006) 1391.

[4] W. Chang, T. Komazu, T. Korenaga, Analytical Letters, 41 (2008) 1468.

[5] R.D. Oleschuk, L.L. Shultz-Lockyear, Y. Ning, D.J. Harrison, Analytical Chemistry, 72 (1999) 585.

[6] J.D. Ramsey, G.E. Collins, Analytical Chemistry, 77 (2005) 6664.

[7] O. Hofmann, D. Che, K.A. Cruickshank, U.R. Müller, Analytical Chemistry, 71 (1998) 678.

[8] J. Wen, E.W. Wilker, M.B. Yaffe, K.F. Jensen, Analytical Chemistry, 82 (2010) 1253.

[9] D. Ross, L.E. Locascio, Analytical Chemistry, 74 (2002) 2556.

[10] S.M. Kim, G.J. Sommer, M.A. Burns, E.F. Hasselbrink, Analytical Chemistry, 78 (2006) 8028.

[11] W.S. Koegler, C.F. Ivory, Journal of Chromatography A, 726 (1996) 229.

[12] K.M. Balss, W.N. Vreeland, P.B. Howell, A.C. Henry, D. Ross, Journal of the American Chemical Society, 126 (2004) 1936.

[13] P.H. Humble, R.T. Kelly, A.T. Woolley, H.D. Tolley, M.L. Lee, Analytical Chemistry, 76 (2004) 5641.

[14] Y.-C. Wang, A.L. Stevens, J. Han, Analytical Chemistry, 77 (2005) 4293.

[15] I. Rubinstein, L. Shtilman, Journal of the Chemical Society, Faraday Transactions 2: Molecular and Chemical Physics, 75 (1979) 231.

[16] I. Rubinstein, Journal of the Chemical Society, Faraday Transactions 2: Molecular and Chemical Physics, 77 (1981) 1595.

[17] I. Rubinstein, Electro-diffusion of ions, Society for Industrial and Applied Mathematics, Philadelphia, 1990.

[18] S.J. Kim, Y.-C. Wang, J.H. Lee, H. Jang, J. Han, Physical Review Letters, 99 (2007) 044501.

[19] D. Stein, M. Kruithof, C. Dekker, Physical Review Letters, 93 (2004) 035901.

[20] N.A. Mishchuk, P.V. Takhistov, Colloids and Surfaces A: Physicochemical and Engineering Aspects, 95 (1995) 119.

[21] F.C. Leinweber, U. Tallarek, Langmuir, 20 (2004) 11637.

[22] A. Plecis, R.B. Schoch, P. Renaud, Nano Letters, 5 (2005) 1147.

[23] K.P. Singh, M. Kumar, Journal of Physical Chemistry C, 115 (2011) 22917.

[24] T. Yasui, N. Kaji, M.R. Mohamadi, Y. Okamoto, M. Tokeshi, Y. Horiike, Y. Baba, ACS Nano, 5 (2011) 7775.

[25] E. Sheridan, D. Hlushkou, R.K. Anand, D.R. Laws, U. Tallarek, R.M. Crooks, Analytical Chemistry, 83 (2011) 6746.

[26] R. Dhopeshwarkar, D. Hlushkou, M. Nguyen, U. Tallarek, R.M. Crooks, Journal of the American Chemical Society, 130 (2008) 10480.

[27] D. Hlushkou, R.K. Perdue, R. Dhopeshwarkar, R.M. Crooks, U. Tallarek, Lab on a Chip, 9 (2009) 1903.

[28] D.R. Laws, D. Hlushkou, R.K. Perdue, U. Tallarek, R.M. Crooks, Analytical Chemistry, 81 (2009) 8923.

[29] R.K. Perdue, D.R. Laws, D. Hlushkou, U. Tallarek, R.M. Crooks, Analytical Chemistry, 81 (2009) 10149.

[30] S.J. Kim, S.H. Ko, K.H. Kang, J. Han, Nature Nanotechnology, 5 (2010) 297.

[31] J. Lee, J. Han, Microfluidics and Nanofluidics, 9 (2010) 973.

[32] F. Mavre, R.K. Anand, D.R. Laws, K.-F. Chow, B.-Y. Chang, J.A. Crooks, R.M. Crooks, Analytical Chemistry, 82 (2010) 8766.

[33] R.K. Anand, E. Sheridan, D. Hlushkou, U. Tallarek, R.M. Crooks, Lab on a Chip, 11 (2011) 518.

[34] R.K. Anand, E. Sheridan, K.N. Knust, R.M. Crooks, Analytical Chemistry, 83 (2011) 2351.

[35] C.-H. Chen, A. Sarkar, Y.-A. Song, M.A. Miller, S.J. Kim, L.G. Griffith, D.A. Lauffenburger, J. Han, Journal of the American Chemical Society, 133 (2011) 10368.

[36] L.F. Cheow, J. Han, Analytical Chemistry, 83 (2011) 7086–7093.

[37] P. Dextras, K.R. Payer, T.P. Burg, S. Wenjiang, W. Ying-Chih, H. Jongyoon, S.R. Manalis, Microelectromechanical Systems, Journal of, 20 (2011) 221.

[38] I. Dumitrescu, R.K. Anand, S.E. Fosdick, R.M. Crooks, Journal of the American Chemical Society, 133 (2011) 4687.

[39] A. Sarkar, J. Han, Lab on a Chip, 11 (2011) 2569.

[40] J.C. McDonald, D.C. Duffy, J.R. Anderson, D.T. Chiu, H. Wu, O.J.A. Schueller, G.M. Whitesides, Electrophoresis, 21 (2000) 27.

[41] J. Monahan, A.A. Gewirth, R.G. Nuzzo, Analytical Chemistry, 73 (2001) 3193.

CHAPTER 4

SUMMARY AND FUTURE DIRECTIONS

1. Summary

The research presented in this dissertation focuses on developing quantitative analytical instrumentation; specifically, we have developed both novel and improved existing analytical instrumentation to quantify small, trace biologically active species from *in vivo* sampling. A broadly versatile and robust immunoassay technique quantified cellular secretions while retaining temporal resolution with segmented flow generated on a microfluidic device.

1.1 Quantitative Immunoassay

A non-destructive competitive immunoassay was developed to be compatible with droplet-based microfluidics. At the bench scale, FPIA is a robust quantitative measure that has been demonstrated to be broadly applicable to a wide variety of analytes including commercial available systems such as Abbot's RDx. While detection of fluorescence anisotropy was previously demonstrated on a microfluidic device, the immunoassay was prepared at the bench scale and not applied to a biological system. As reported (see Chapter 2), we optimized an FPIA for use in monitoring insulin secretions

from on-chip cultured Islet of Langerhans with a 5 nM detection limit and dynamic range up to 1 uM. Temporal resolution of perfusion sampling was retained by immediate segmentation of flow on-chip into water-in-oil droplet; moreover, segmented flow was both experimentally and numerically demonstrated to improve the temporal resolution of two orders of magnitude such that sub-minute oscillations in glucose stimulate insulin release were observed in some experiments. While the specific antibody-antigen complex will affect the detection limit and dynamic range of the FPIA, this system serves as a model for neuropeptide quantification.

1.2 On-chip Preconcentration of Analytes

Preconcentration of fluorescently labeled insulin in highly ionic media was demonstrated via ICP induced by a potential applied across a microfluidic channel with a BPE. While ICP has been previously demonstrated to enrich samples by factors as high as one-million-fold, we report a robust BPE preconcentator that is compatible with highly ionic media. This in-line precocentration of insulin resulted in enrichment factors as high as 50,000-fold in an hour. While insulin was larger than many neuropeptides in mass, both have similar electrostatic charge and electrophoretic mobility (within an order of magnitude) such that it serves as a model system for neuropeptide quantification. Water-in-oil droplet segmentation was generated on-demand to prevent dilution by dispersion; specifically, droplets generated at or greater than 10 nL captured the concentrated band with greater than 90% efficiency. This preconcentration and droplet sequestration device was compatible with the FPIA quantification system discussed above.

2. Future Directions

The microfluidic devices developed in this dissertation were compatible with microdialysis sampling of neuropeptides. In future work, these preconcentration and FPIA detection devices may be integrated together with microdialysis sampling. While microdialysis sampling recovers analytes at low concentrations when operated at high flow rates, this lower concentration improves mass sensitivity. Specifically, both the higher flux of analytes through the BPE device and higher rate of enrichment for more dilute analytes decrease the time to reach the nM detection limits of the FPIA. Concentration with BPE may also be multiplexed such that while a volume of sample is preconcentrated, another volume is simultaneously collected.

Several neuropeptides, namely opioid peptides, are of interest in the study of several disease states such as Parkinson's disease as well as to function in signaling pathways of pain and reward. The integrated microfluidic device described above offers a low cost method of in-line quantification of these and other neurotransmitters in microdialysis sampling for rodent models.

Optimization of preconcentration and droplet sequestration by modification of the location of the oil channels to decrease to final droplet volume additionally offers improvements in capture efficiency. These improvements in capture efficiency increase the final concentration in the droplet such that the nM detection limits of the FPIA would be achieved in shorter concentration timescales. Droplet based FPIA quantification offers a promising on-chip detection of small biologically relevant species.

APPENDIX A

FLOUROGENIC ENZYMATIC QUANTIFICATION OF GLUCOSE AND FINITE ELEMENT METHOD MODELING OF MASS TRANSPORT AND FLUIDICS OF *IN VIVO* MICRODIALYSIS SAMPLING

1. Context

In an effort to develop a quantitative analysis that would be compatible with microdialysis sampling, water-in-oil droplet storage and non-destructive analysis a variety of techniques were investigated including enzymatic fluorogenic analysis. A bench-scale quantitative assay was optimized for biologically relevant concentrations of glucose prior modifications made for on-chip analysis. The effect of membrane thickness, probe size and flow rate were numerically modeled with the finite element method commercially available software suite COMSOL. Numerical and experimental results were compared to determine the relative contributions from the three parameters discussed above. The sections (excerpts) below were previously reported both in M Wang's dissertation and a published manuscript ("Improved Temporal Resolution for in Vivo Microdialysis by Using Segmented Flow" by Meng Wang, Gregory T. Roman, Kristin Schultz, Colin Jennings, and Robert T. Kennedy in Analytical Chemistry, 80 (2008) 5607-5615):

2. Background

Microdialysis sampling is widely used for in vivo monitoring of chemicals in extracellular space of tissues such as heart, fat, liver, and brain [1-3]. In chemical monitoring applications, temporal resolution is a key figure of merit because analyte concentrations can change rapidly [4-6]. When using microdialysis sampling, temporal resolution is usually limited by mass sensitivity of the analytical method coupled to the probe i.e., sample must be collected long enough to obtain a detectable quantity. When techniques such as HPLC are used, the temporal resolution is often 10-30 min [7]; however, coupling microdialysis to nanoscale analytical techniques such as capillary electrophoresis (CE), microbore liquid chromatography (LC), and electrochemical sensors have shortened sampling times to seconds [4, 8-18].

When using high sensitivity analytical methods, other factors can begin to limit temporal resolution achievable with microdialysis sampling. One inherent limitation is broadening of sample zones due to Taylor dispersion as they are transferred from sampling probe to analytical system [19]. The effect of Taylor dispersion can be ameliorated by using high flow rate through the probe; however, this decreases relative recovery thus decreasing the concentration of analytes measured. Higher flow rates are also incompatible with smaller probes and alternative sampling methods such as low flow push-pull perfusion [20] or direct sampling [21] that improve spatial resolution. Taylor dispersion can also be decreased by shortening the length of tubing connections; however, this approach is impractical for experiments involving freely moving animals. Thus, although temporal resolution of 3 s has been described for sampling from an anesthetized animal at high dialysis flow rates; temporal resolution is increased to 90 s

for low flow rates or work with awake and freely moving animals [16]. In this work, we describe coupling microdialysis probes to a microfluidic segmented flow system to avoid these limitations. Segmented flow can eliminate Taylor dispersion by localizing samples as aqueous droplets or plugs formed in a stream of water-immiscible carrier fluid [22-25].

A surge of recent research into segmented flows has shown the potential of this approach for chemical measurement. Droplets or plugs from femtoliter to microliter volume can be reproducibly created using a variety of microfluidic geometries including tee junctions [26], Y-junctions [23], and nozzles [27]. Furthermore, plugs can be manipulated for chemical analysis through reagent addition [28-30], rapid on-chip mixing [29-30], and transfer to outside tubing [29-32]. Recent applications of such systems include kinetic measurement [26, 33], synthesis [29, 34-35], protein crystallization [32, 36], DNA analysis [37], PCR [38], cell sorting [39] and cell encapsulation [23, 40]. Although avoiding dispersion or mixing of discrete samples is often cited as an advantage of segmented flow, this approach has not been described for chemical monitoring applications such as in vivo microdialysis.

The goal of this study was to combine in vivo microdialysis sampling with a segmented flow microfluidic device to conserve temporal resolution while sample plugs were transported from the probe to a downstream detection system. We determined conditions for obtaining dialysate flow segmentation on the scale needed for in vivo analysis, tested the effects of flow segmentation on temporal resolution, and demonstrated use of the system for analytical measurements by coupling it to an on-line enzyme assay for monitoring glucose in the brain of living rats. We demonstrate that

temporal resolution of 15 s is possible and that this resolution is independent of both time to transport sample to the analytical system and dialysis flow rate.

3. Materials and Methods

3.1 Chemicals and Reagents

All chemicals were used as received. Perfluorodecalin, fluorescein, hexamethyldisilazane (HMDS), octadecyltrichlorosilane (OTCS), n-hexadecane, and methanol were purchased from Sigma-Aldrich (St. Louis, MO). Salts for artificial cerebral spinal fluid (aCSF) were purchased from Fisher Scientific (Chicago, IL). A glucose assay kit consisting of Amplex® red reagent, dimethylsulfoxide (DMSO), horseradish peroxidase (HRP), glucose oxidase (GOX), D-glucose, concentrated reaction buffer (0.05 M sodium phosphate, pH 7.4), and H_2O_2 was purchased from Invitrogen (Carlsbad, CA). All aqueous solutions were prepared with water purified and deionized to 18 MΩ resistivity using a Series 1090 E-pure system (Barnstead|Thermolyne Cooperation, Dubuque, IA).

3.2 LIF Detection and Data Analysis

For visual inspection and monitoring of sample plugs, the chip or collection capillary was mounted on a Nikon inverted microscope (Eclipse TS100, Melville, NY). Photographs were taken through the microscope using a digital camera (FinePix F30, Fujifilm, Japan). When detecting fluorescence, the collection capillary or chip was mounted on an epi-illumination inverted microscope (Axiovert 100, Carl Zeiss Inc.). Fluorescence was excited using a 488 nm line of an Ar^+ laser (Melles Griot, Carlsbad,

CA) for fluorescein or the 543.5 nm line of a He-Ne laser (Melles Griot, Carlsbad, CA) for Amplex® red. Fluorescence was collected through a 10x objective through appropriate filter sets and detected using a photometer (R3896, Hamamatsu Photonics, Bridgewater, NJ) mounted on the microscope. The photometer was set to low pass filter at 250 Hz. Fluorescence signals were collected via a data acquisition card (PCI-6036E, National Instruments, Austin, TX) at 1000 Hz using LabView program written in-house. Microsoft Excel 2007 (Microsoft, Redmond, WA), Igor Pro 6.01 (Wavemetrics, Inc., Lake Oswego, OR), and Cutter 7.0 [50] were used for data analysis and graphing.

3.3 Computational Modeling of Microdialysis Sampling

Microdialysis probe sampling dynamics were modeled using COMSOL Multiphysics ® 3.3 (Comsol, Inc., Burlington, MA). 1 and 2 mm long probes were approximated as 200 μm wide cylinders with a 40 μm i.d. by 100 mm o.d. capillary inserted to within 50 μm of the bottom of the probe, a similar capillary outlet at the top of the probe and a 10 μm thick membrane. The boundary layer (i.e., quiescent solution) around the probe was approximated to be 50 μm thick for a well stirred solution (assuming $R_e \sim 100$) [51]. Diffusion was treated as uniform throughout the boundary layer, membrane and probe volume. All models were solved in three dimensions by modeling mass transport from the edge of the boundary layer into the perfusing flow into the probe as a function of time for 1 minute. The net concentration out of the probe was fit to a Hill equation by nonlinear regression using Origin® 6.0 (Microcal Software, Inc., Northhampton, MA) to generate data traces. The outlet capillary from the probe was modeled as a 3.5 cm long by 40 μm i.d. capillary in two dimensions. Analyte

concentration and response times were determined from the time-dependent concentration profile at the end of the capillary model. Constants used in the model were 4.25×10^{-6} cm^2/s as diffusion coefficient for fluorescein [52], 993 kg/m^3 for density of water, and 6.90×10^{-4} Pa s for viscosity of water (37 ^oC). Specifically, fluidic domains were solve first by setting outlet pressure to neutral and the inlet at a constant flow rate (either 0.2 or 2 μL/min depending on experiment). Using the values stored from these results as constants, convection and diffusion was then modeled for 1 min with 0.01 s time steps by setting the inlet concentration at zero and holding the concentration at the outside of the boundary layer as 1 unit. This process was first applied to the bottom section (slice) of the probe model and then repeated for each section above but fitting six concentric rings with the method described above from the outlets of the previous model. Concentration profile as a function of time was plotted in the figure below for both 1 and 2 mm probes and at both 0.2 and 2 μL/min flow rates.

3.4 In Vitro Glucose Assay

Glucose assays were performed on-line by mixing reagents and dialysate within a chip to form sample plugs that were pumped to a detection zone in a collection capillary downstream of the mixing/plug formation point. Reagents were prepared from stock solutions of Amplex® red (10 mM in DMSO), GOX (100 UI/mL in 0.05 M sodium phosphate reaction buffer, pH 7.4) and HRP (10 UI/mL in reaction buffer, as described above) according to vendor instructions. Stock solution was stored frozen at -80 ^oC as single-use aliquots. For each day's experiment, stock solution aliquots were thawed on ice and then diluted with reaction buffer to produce separate enzyme (6 UI/mL GOX and

0.6 UI/mL HRP) and indicator (0.3 mM Amplex® red) solutions. These working solutions were kept on ice and shielded from light by aluminum foil at all times. To ensure activity of reagents, solutions were replaced every two hours.

For on-line glucose assay, the aqueous inlet channel shown in Figure A.1A was modified to have 3 channels (one for HRP/GOX solution, one for Amplex® red solution, and one for dialysate) that merged to a single channel just before the tee intersection (details given in text). The flow rate for sample stream was 200 nL/min and for each reagent stream 50 nL/min. Oil flow rate was 1000 nL/min. With these flow rates, each plug was expected to contain the concentrations recommended by the vendor, i.e. 0.1 UI/mL HRP, 1 UI/mL GOX and 50 mM Amplex® red. To test and calibrate the on-line assay, glucose solutions with concentrations ranging from 0.1 mM to 5 mM were prepared in aCSF and sampled by microdialysis. Fluorescence of each resulting sample plug was detected 40 cm downstream using LIF as described above.

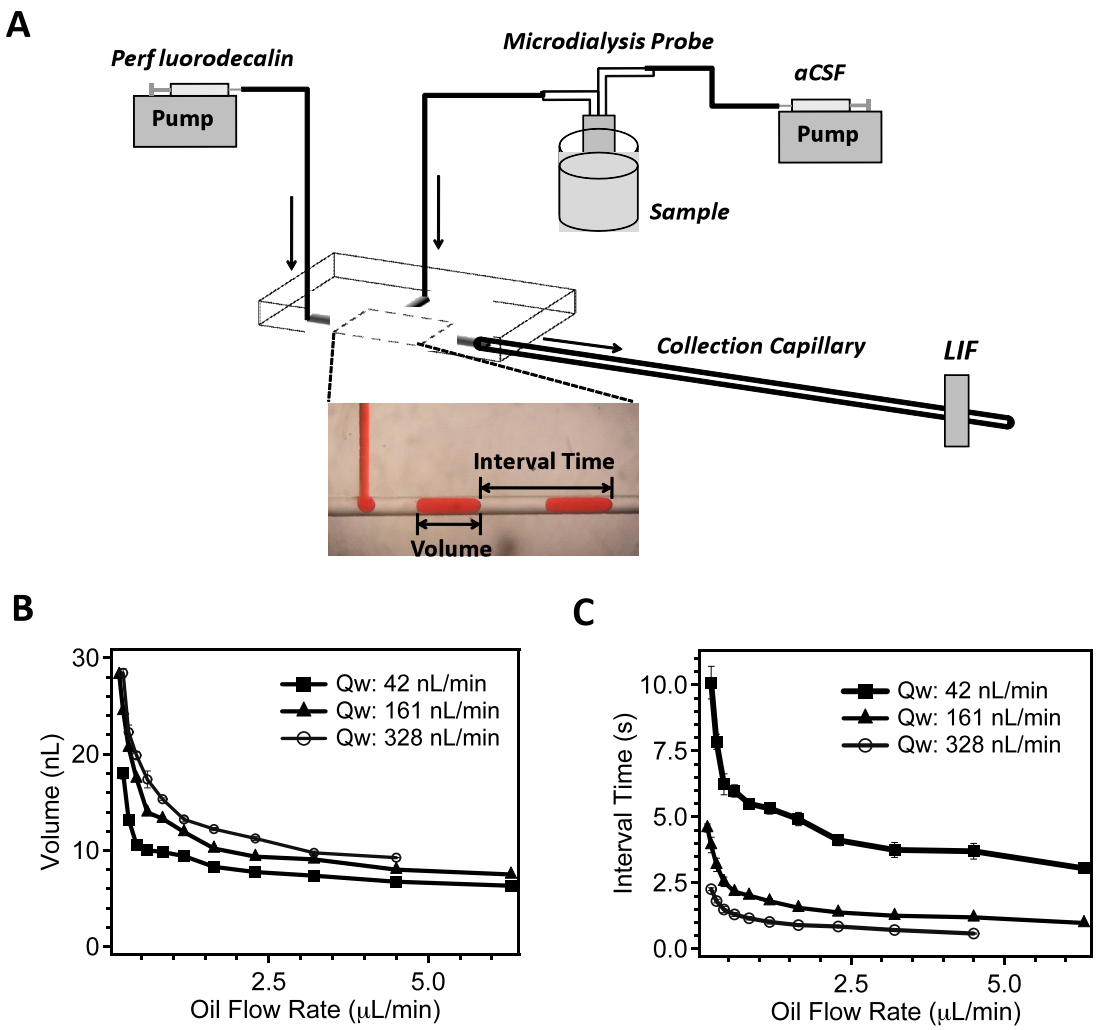

Figure A.1. (A) Illustration of microdialysis/segmented flow system used in this work. Arrows indicate direction of flow. Micrograph in inset illustrates plug generation at a tee junction. (Aqueous stream contains food dye for visualization.) Aqueous channels had a width of 125 mm and main channel with segmented flow had a width of 250 mm. (B) Dependence of plug volume on oil flow rate at different aqueous flow rates (Q_w) for structure shown in Figure A.1A. (C) Dependence of interval time between plugs on oil flow rate at Q_w for structure shown in Figure A.1A.

4. Results and Discussion

4.1 Effect of Flow Rates on Plug Volume and Time Interval

In a sampling system with on-line analysis that uses segmented flow, the sample plug volume, interval between plugs, and plug generation frequency have a large impact on both the temporal information that can be obtained and the analytical methods that should be adopted. The sample plugs must be large enough that the amount of analyte in them is higher than the mass detection limits of the analytical method. Sample plug generation frequency sets the upper limit to temporal resolution obtainable, e.g. a system that generates one sample plug every 10 s will have a temporal resolution no higher than 10 s. If on-line analysis is used, then the interval between plugs that are created must be longer than the minimum time required for each analysis (e.g., separation time in LC). In this work we used a microfluidic tee to segment flow from the dialysis probe. As demonstrated previously [54-55], plugs generated in a tee can be controlled by changing relative flow rates of the sample and carrier fluid as well as dimensions of the channels. Although models have been developed to predict plug generation,[54] we found that experimentation was required to obtain the desired plug formation dynamics.

For this work, we sought to generate plugs from sample stream flow rates in the 0.1 to 1 mL/min range at 1 to 10 s intervals to yield samples with low nanoliter volumes. This flow rate is typical for microdialysis and the plug formation frequency represents significant improvement in temporal resolution while generating plugs that are easily manipulated and analyzed. As shown in Figure A.1, a tee with 125 × 80 mm inlet channel and 250 × 80 mm main channel allowed such plugs to be formed. For a given sample flow rate, increasing the oil flow rate decreased plug volumes and intervals

(Figure A.1B and A.1C). Decreasing the sample flow rate generated smaller plugs at longer intervals. The dynamic range of intervals was approximately 0.6 to 10 s. Plugs were reproducible with < 5% RSD in volume and < 8% RSD in interval time. Chip dimensions could also be varied to yield different ranges that might be appropriate for different applications. For example, with 50 × 12 mm channels we generated plugs of 50 to 200 pL at < 1 s intervals. In some cases, it may be desirable to independently control sample size and interval between plugs; however, this is not possible with the tee junction. An active system where plugs are formed by a trigger would allow such independent control but would also necessitate a more complex instrument.

4.2 Conservation of Temporal Resolution with Segmented Flow System

After demonstrating controlled sample plug formation, we tested the potential to preserve temporal resolution in comparison to a continuous flow system during microdialysis sampling. For these experiments, step changes in fluorescein concentration were made at the probe surface while recording response curves by LIF detection. A dialysis flow rate of 200 nL/min was used representing a relatively low flow rate that generates high relative recovery (approximately 53% for glucose) but is usually not associated with good temporal resolution. For the continuous flow system the oil flow was replaced by aCSF. Recordings were made both near the tee junction and 40 cm downstream for both continuous flow and segmented flow (see Figure A.2A and A.2B). A comparison between upstream and downstream response curves for both systems demonstrates the advantage of segmented flow over continuous flow for conserving temporal resolution. (Temporal resolution and response time in this discussion refer to

the time from the initial increase in signal to the steady state signal and does not include the delay time associated with flowing from the probe to the detection window.) With segmented flow, on-chip and downstream detection produced response curves that exactly overlapped (Figure A.2C), verifying prevention of axial dispersion between plugs and conservation of temporal resolution after sampling. In contrast, severe deterioration in temporal resolution, represented as a broadened transition zone, was observed with continuous flow (Figure A.2D), due to axial dispersion of sample zones during transport at low flow rate through a capillary.

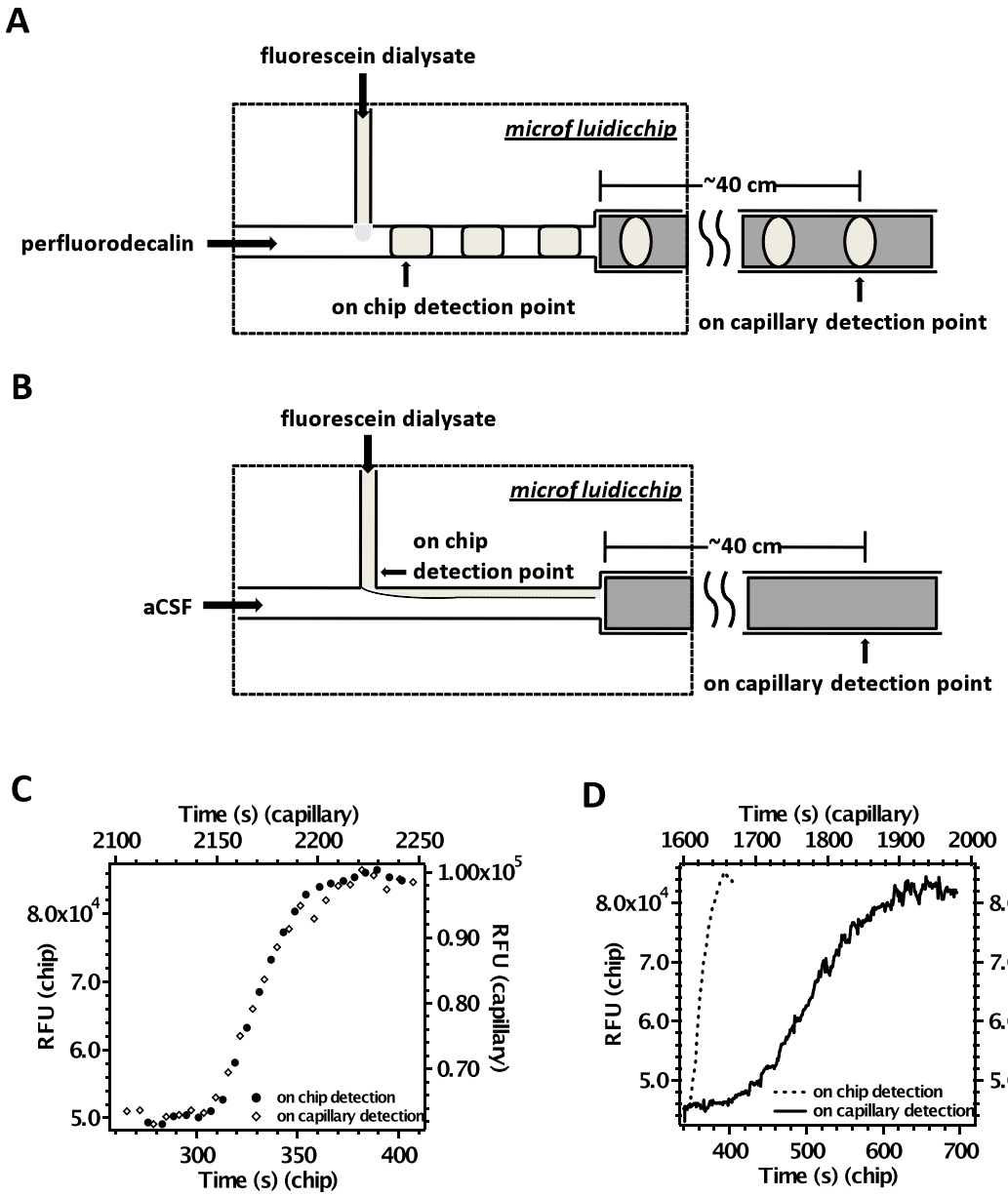

Figure A.2. Illustration of on chip and on capillary detection points for comparing temporal resolution of segmented flow (A) and continuous flow (B) systems. Step change of fluorescein concentration from 50 nM to 100 nM was made at the probe surface and response curves at the two detection points were recorded for segmented flow (C) and continuous flow (D). For (C), the data points represent the maximal fluorescence recorded from each sample plug as it passed through the detector. The top time axis is for the downstream (capillary) detection point and the bottom for the on-chip detection point in both graphs.

Sampling flow rate was 200 nL/min and cross-sectional flow rate (perfluorodecalin or aCSF) was 1 mL/min. Microfluidic chip conditions were the same as described in Figure A.1.

We next explored the upper limits of temporal resolution with this system. To do this, we repeated the step change experiment but with stirred solutions and probes equilibrated to 37 ^{o}C. Stirring is expected to decrease the distance required for analyte to diffuse to the probe while the elevated temperature increases diffusion coefficients. Using this approach we observed response times of ~ 30 s (time from 10-90% of maximal signal) at 200 nL/min dialysis flow rates (see Figure A.3A). Increasing the dialysis flow rate to 1 mL/min did not improve the temporal resolution (Figure A.3B). Decreasing the dialysis probe length by half to 1 mm resulted in an approximately 2-fold improvement in response time to 15 s at both flow rates (Figure A.3C and A.3D). Thus, response time scaled with membrane length rather than flow rate. These results suggest that mass transport across the membrane, and not Taylor dispersion, limits temporal resolution under these conditions.

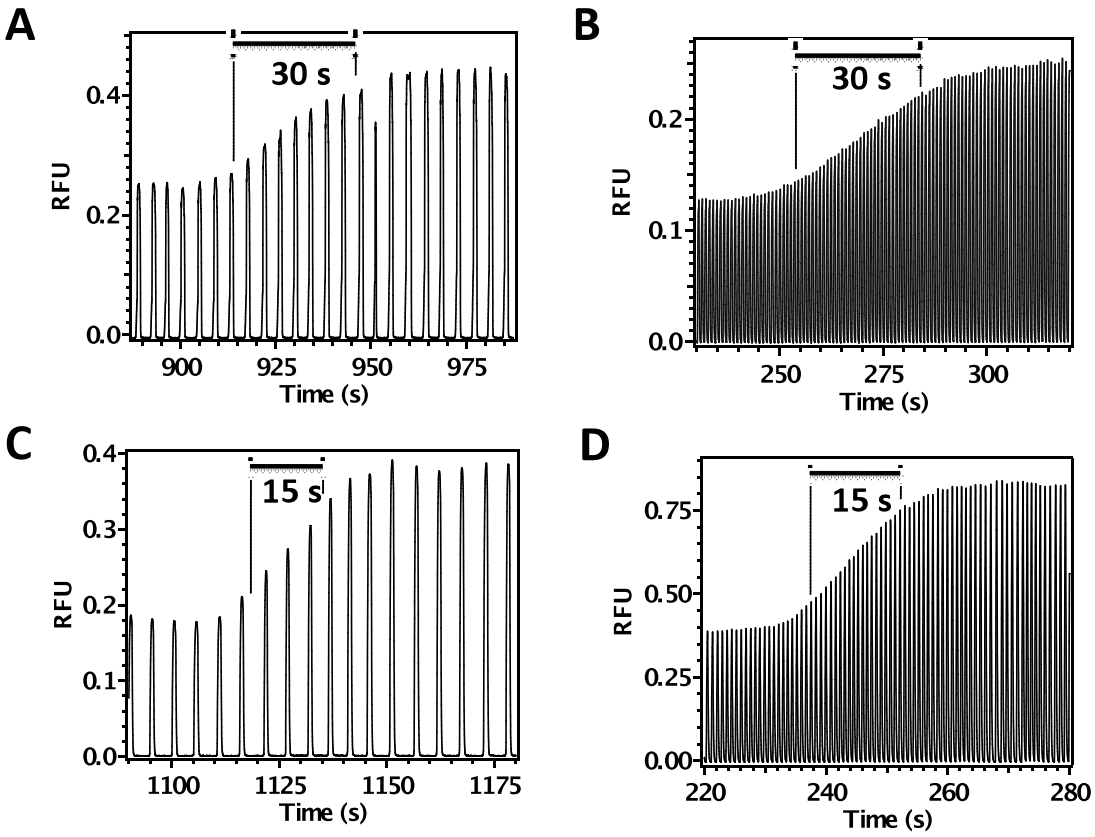

Figure A.3. Response obtained at both low and high sampling flow rate with microdialysis probes with different membrane lengths. (A) 2 mm probe at 200 nL/min; (B) 2 mm probe at 1 mL/min; (C) 1 mm probe at 200 nL/min; (D) 1 mm probe at 1 mL/min. Fluorescein concentration was changed from 2 mM to 5 mM at the probe surface. Cross-sectional flow rates were 1 mL/min for 200 nL/min sampling rate and were 4 mL/min for 1 mL/min sampling rate. Data traces are raw output from LIF detector and show detection of individual sample plugs. Temporal resolution, defined as the time during which signals increased from 10% to 90% of the maximum intensity, is marked on each graph. Chip conditions were the same as described in Figure A.1.

To further explore this effect, we modeled the response of a dialysis probe to step changes in concentration in a stirred solution at 37 ^{o}C. The model was based on the geometry of the probe (see Experimental section and Figure A.4A). The system was considered to have a 50 mm boundary layer and diffusion coefficient within the

membrane was considered to be the same as solution. These conservative estimates have the effect of making observed responses limited primarily by flow and diffusion within the probe and tubing and not transport across the membrane. As shown in Figure A.4, this model predicts response times of 11.9 s for a 2 mm probe at 0.2 mL/min. Increasing the flow rate to 1 mL/min decreased the response time to 3.5 s. Cutting the probe length in half yielded a small decrease in response time to 8.0 and 2.1 s with 0.2 and 1 mL/min flow rates, respectively. Thus, when the transport across the membrane is not limiting, the response times are 2 to 8-fold faster than those measured experimentally. Furthermore, in contrast to experimental results, the dialysis flow rate has a bigger effect on response time than membrane length. This result further supports the conclusion that transport across the membrane is a limiting factor in response time in this system. Lower effective diffusion coefficients within the membrane [19, 56], adsorption to the membrane, and flow leakage through the membrane are all factors that can slow transport and therefore alter response time. Accurate knowledge of these processes would be required to correctly predict response times. This work suggests that improved membranes or sampling without membranes, such as direct [21] or push-pull sampling [20], would be required to further improve the temporal resolution.

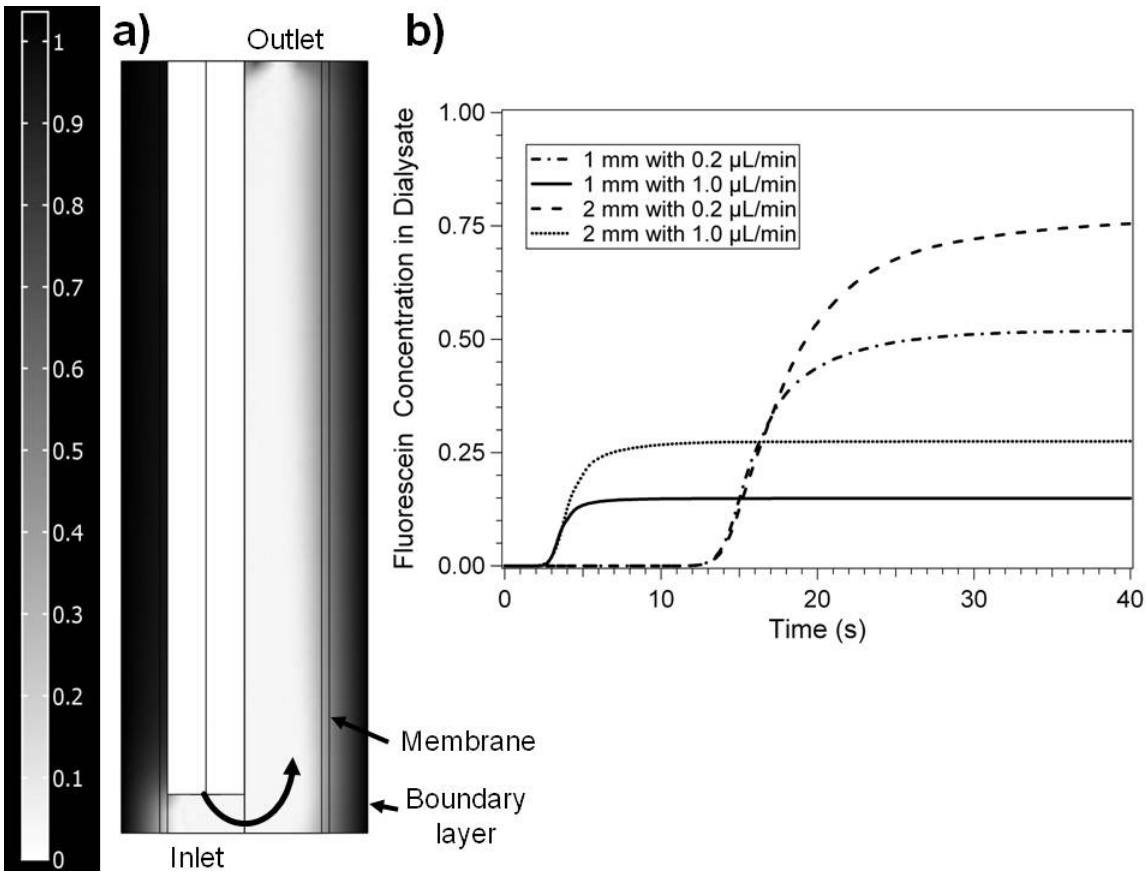

Figure A.4. Simulation of response to step change in fluorescein concentration at a microdialysis probe using COMSOL. (A) The geometry of the dialysis probe was the same as those used experimentally i.e., 200 mm inner diameter, 220 mm outer diameter, side-by-side inlet and outlet capillaries and a 40 mm i.d. by 3.5 cm long exit capillary. Curved arrow indicates direction of dialysis flow. The steady state concentration gradient for unit concentration outside the probe is shown over the geometry in this illustration. (B) The response shown is the concentration change at the outlet of the exit capillary following a step change from zero to unit concentration at time zero. The probe lengths and dialysis flow rates are given in the legend.

4.3 On-Chip Glucose Assay with Segmented Flow

To demonstrate the potential of the microdialysis to segmented flow system for chemical analysis, we integrated an on-line glucose enzyme assay. The sampling chip was modified with a triple-branch inlet to enable addition of assay reagents to the sample

stream 1 mm upstream of the plug formation point. As illustrated in Figure A.5A, sample stream from the microdialysis probe flowed in the middle branch while enzymes (GOX, HRP) and dye (Amplex® red) were infused from the two side branches. Sample stream flow rate was 200 nL/min while the reagent stream flows were 50 nL/min each. This net flow rate resulted in sample plugs forming at 4 s intervals. Mixing and enzymatic reaction took place to form a fluorescent product (see Figure A.5B for reaction scheme) within plugs as they were transported in a capillary from the microfluidic chip to detection window. Reaction time could be adjusted by varying the length of the capillary as well as oil flow rate. Although the assay kit suggested a 30 min incubation time before detection, we found that 17 min was enough to distinguish different glucose concentrations. This reaction time could be achieved by a 40 cm capillary at 1 mL/min oil flow rate. An illustration of the raw fluorescence signal from the plug enzyme assay at the detection point during a step change from 0.2 to 1 mM glucose is shown in Figure A.5C. This trace illustrates the uniformity of signal intensities across different plugs for a given glucose concentration. Indeed, the assay yielded 2.3% RSD (n = 56) at 1 mM glucose. The assay also had a linear response up to 2 mM glucose and a detection limit of 50 mM glucose (see Figure A.5D). The trace in 5C also illustrates the preservation of temporal resolution for this experiment even though the sample plugs required 17 min for transport from the sampling to detection points. This effect represents a substantial advantage of the segmented flow system for assays that require long reaction times. This result further illustrates that the segmented flow system can maintain temporal resolution regardless of downstream processes.

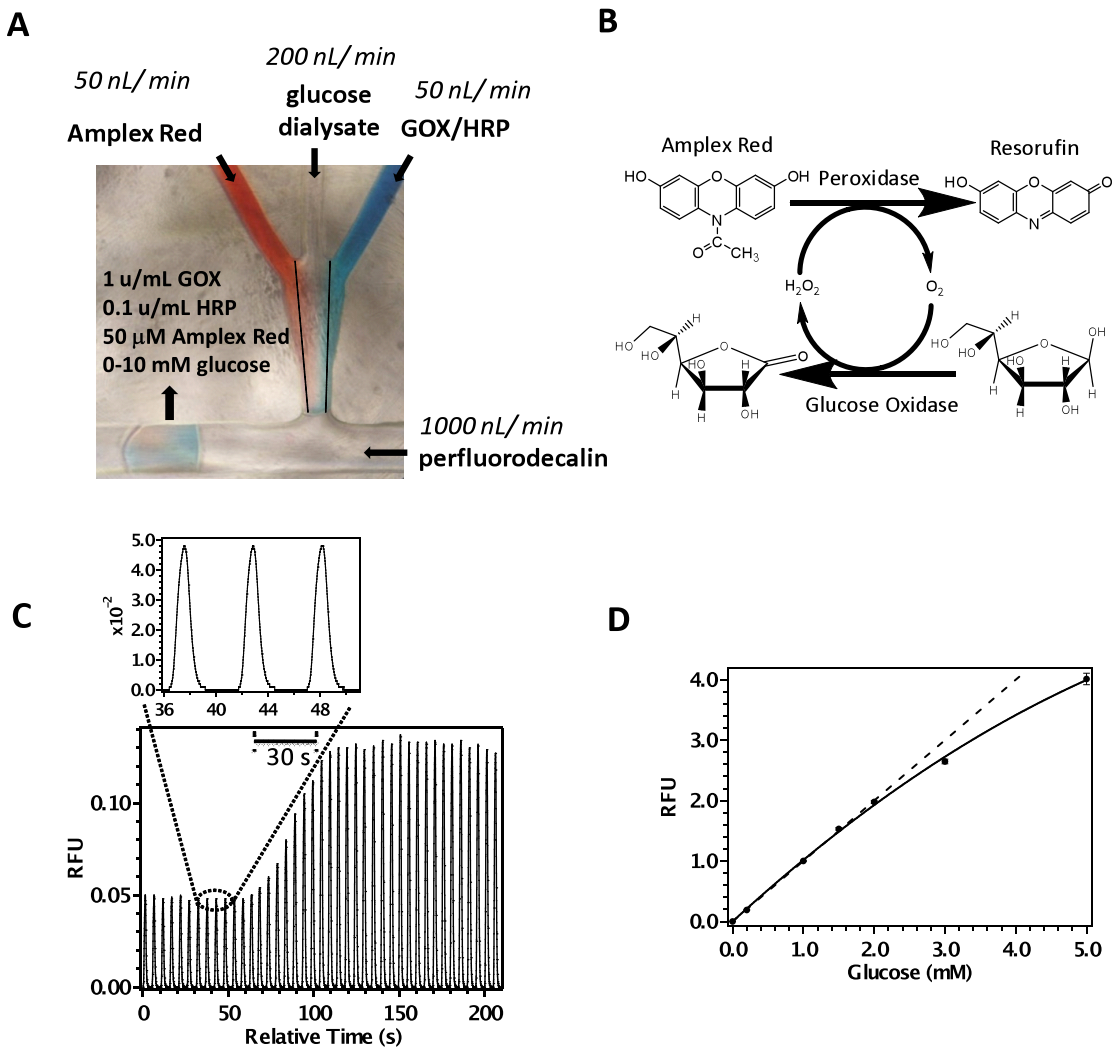

Figure A.5. Glucose assay with segmented flow system. (A) Micrograph of microchannel network used for enzymatic assay within plugs. Food dye has been added to the Amplex® red and GOX/HRP streams for visualization. (B) Reaction scheme for the enzymatic assay. (C) LIF response when glucose concentration was changed at the probe from 0.2 to 1 mM. The inset shows an amplified view of the trace. Data are raw traces showing detection of individual plugs. (D) Calibration curve for glucose sampled by microdialysis and assayed using this system. Glucose concentrations are sampled concentrations.

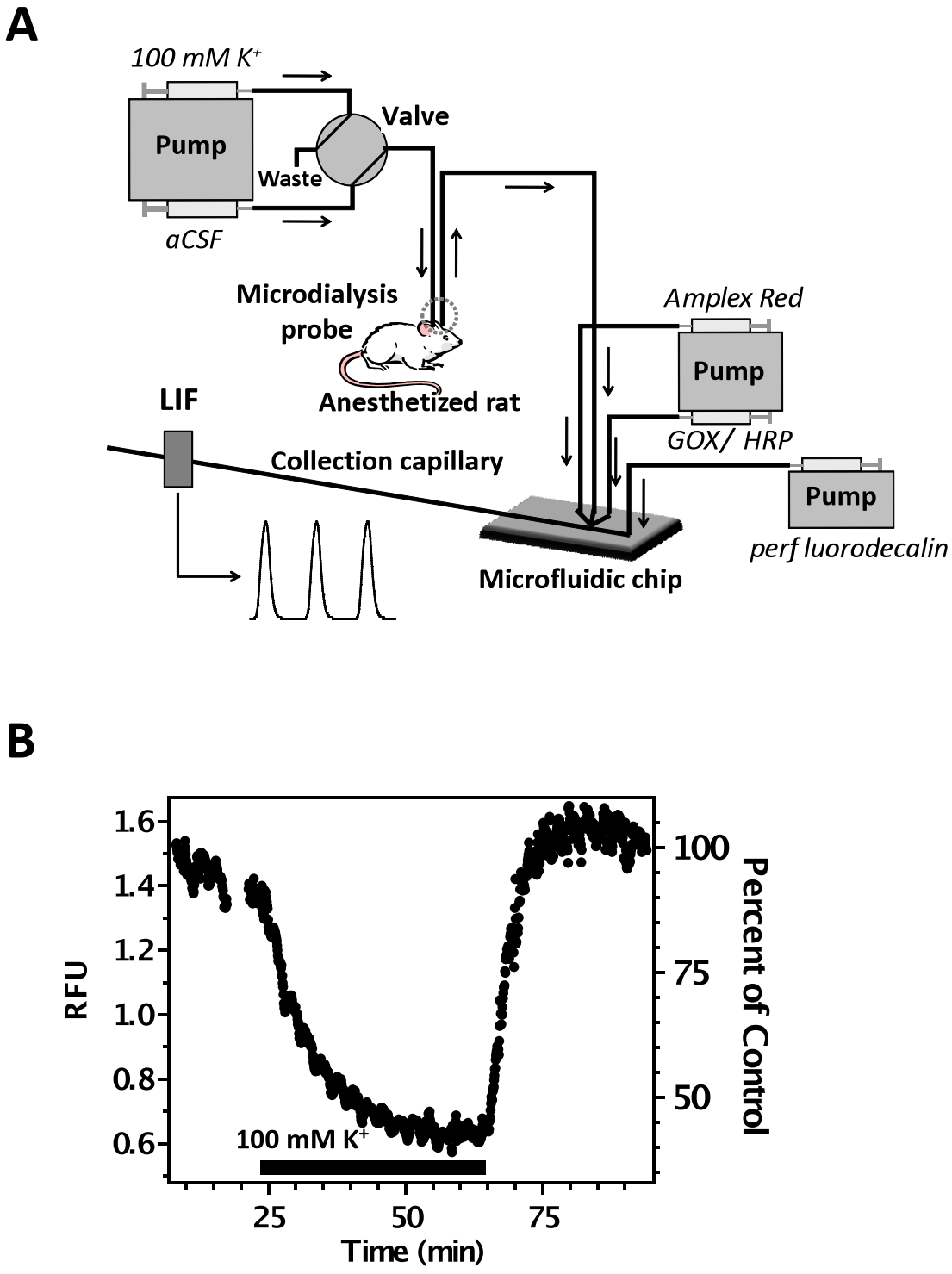

Figure A.6. (A) Overview of system for in vivo glucose assay. (B) Time course of extracellular glucose concentration in the NAC of rats infused high K^+ (100 mM) aCSF through the probe. Time on axis is time since switch was made to high K^+. Black bar indicates application of K^+ corrected dead volume of system.

Axis on the left is relative fluorescence unit (RFU) for the maximal signal in each plug while right axis expresses data as the percentage of basal glucose concentration.

5. Conclusion

Segmented flows have received significant attention in chemical analysis in recent years primarily for their potential in high-throughput analysis. In this paper, we reduce to practice the possibility that microfluidic segmented flows can be used to prevent temporal distortion in a sampling and monitoring experiment. Temporal resolution for microdialysis was maintained at 15 s regardless of downstream processes thus allowing good temporal resolution to be maintained for experiments requiring long connection capillaries (such as freely moving animals) or assays that involve long reaction times. The use of segmented flow with sampling represents a significant advance for sampling approaches because it decouples analysis time from the temporal resolution that is possible. It also provides a convenient approach for manipulating nanoliter volume fractions that are generated with performing high temporal resolution measurements. Our experiments suggest that future research aimed at improving temporal resolution should be directed towards improving sampling processes. Furthermore, coupling to other assay systems will be important in allowing this approach to extend beyond enzyme assays. Extension of the method to other assays and coupled to different sampling probes will likely yield systems with temporal resolution that approaches that of many sensors.

References

(1) Plock, N.; Kloft, C. European Journal of Pharmaceutical Science, 25 (2005**)** 1-24.

(2) Ungerstedt, U. Measurement of neurotransmitter release in vivo; John Wiley and Sons: New York, 1984.

(3) Ungerstedt, U.; Pycock, C. Bulletin der Schweizerischen Akademie der Medizinischen Wissenschaften, 30 (1974) 44-55.

(4) Chen, A.; Lunte, C. E. Journal of Chromatography A, 691 (1995) 29-35.

(5) During, M. J. Microdialysis in the neurosciences; Elsevier Science Publishers BV: New York, 1991.

(6) Wages, S. A.; H., C. W.; Justice, J. B. J. Analytical Chemistry, 58 (1986) 1649-1656.

(7) Watson, C. J.; Venton, B. J.; Kennedy, R. T. Analytical Chemistry, 78 (2006) 1391-1399.

(8) Bert, L.; Parrot, S.; Robert, F.; Desvignes, C.; Denoroy, L.; Suaud-Chagny, M. F.; Renaud, B. Neuropharmacology, 43 (2002) 825-835.

(9) Bert, L.; Robert, F.; Denoroy, L.; Stoppini, L.; Renaud, B. Journal of Chromatography A, 755 (1996) 99-111.

(10) Bowser, M. T.; Kennedy, R. T. Electrophoresis, 22 (2001) 3668-3676.

(11) Boyd, B. W.; Witowski, S. R.; Kennedy, R. T. Analytical Chemistry, 72 (2000) 865-871.

(12) Church, W. H.; Justice, J. B. J. Analytical Chemistry, 59 (1987) 712-716.

(13) Davies, M. I.; Cooper, J. D.; Desmond, S. S.; Lunte, C. E.; Lunte, S. M. Advances in Drug Delivery Review, 45 (2000) 169-188.

(14) Hernandez, L.; Tucci, S.; Guzman, N.; Paez, X. Journal of Chromatography A, 652 (1993) 393-398.

(15) Kennedy, R. T.; Watson, C. J.; Haskins, W. E.; Powell, D. H.; Strecker, R. E. Current Opinions in Chemical Biology, 6 (2002) 659-665.

(16) Lada, M. W.; Vickroy, T. W.; Kennedy, R. T. Analytical Chemistry, 69 (1997) 4560-4565.

(17) Tucci, S.; Rada, P.; Sepulveda, M. J.; Hernandez, L. Journal of Chromatography B Biomedical Science Applications, 694 (1997) 343-349.

(18) Parkin, M.; Hopwood, S.; Jones, D. A.; Hashemi, P.; Landolt, H.; Fabricius, M.; Lauritzen, M.; Boutelle, M. G.; Strong, A. J. Journal of Cerebral Blood Flow and Metabolism, 25 (2005) 402-413.

(19) Norton, L. W.; Yuan, F.; Reichert, W. M. Analytical Chemistry, 79 (2007) 445-452.

(20) Kottegoda, S.; Shaik, I.; Shippy, S. A. Journal of Neuroscience Methods, 121 (2002) 93-101.

(21) Kennedy, R. T.; Thompson, J. E.; Vickroy, T. W. Journal of Neuroscience Methods, 114 (2002) 39-49.

(22) Gunther, A.; Jensen, K. F. Lab on a Chip, 6 (2006) 1487-1503.

(23) Gunther, A.; Thalmann, M.; Jhunjhunwala, M.; Schmidt, M. A.; Jensen, K. F. Langmuir, 21 (2005) 1547-1555.

(24) Gunther, A.; Khan, S. A.; Thalmann, M.; Trachsel, F.; Jensen, K. F. Lab on a Chip, 4 (2004) 278-286.

(25) Kralj, J. G.; Sahoo, H. R.; Jensen, K. F. Lab on a Chip, 7 (2007) 256-263.

(26) Song, H.; Tice, J. D.; Ismagilov, R. F. Angewandte Chemie International Edition, 42 (2003) 768-772.

(27) Shim, J. u.; Cristobal, G.; Link, D. R.; Thorsen, T.; Jia, Y.; Piattelli, K.; Fraden, S. Journal of the American Chemical Society, 19 (2007) 8825-8835.

(28) Li, L.; Boedicker, J. Q.; Ismagilov, R. F. Analytical Chemistry, 79 (2007) 2756-2761.

(29) Shestopalov, I.; Tice, J. D.; Ismagilov, R. F. Lab on a Chip, 4 (2004) 316-321.

(30) Song, H.; Li, H. W.; Munson, M. S.; Van Ha, T. G.; Ismagilov, R. F. Analytical Chemistry, 78 (2006) 4839-4849.

(31) Zheng, B.; Ismagilov, R. F. Angewandte Chemie International Edition, 44 (2005) 2520-2523.

(32) Zheng, B.; Tice, J. D.; Roach, L. S.; Ismagilov, R. F. Angewandte Chemie International Edition, 43 (2004) 2508-2511.

(33) Gerdts, C. J.; Sharoyan, D. E.; Ismagilov, R. F. Journal of the American Chemical Society, 126 (2004) 6327-6331.

(34) Chan, E. M.; Alivisatos, A. P.; Mathies, R. A. Journal of the American Chemical Society, 127 (2005) 13854-13861.

(35) Khan, S. A.; Gunther, A.; Schmidt, M. A.; Jensen, K. F. Langmuir, 20 (2004) 8604-8611.

(36) Zheng, B.; Roach, L. S.; Ismagilov, R. F. Journal of the American Chemical Society, 125 (2003) 11170-11171.

(37) Burns, M. A.; Johnson, B. N.; Brahmasandra, S. N.; Handique, K.; Webster, J. R.; Krishnan, M.; Sammarco, T. S.; Man, P. M.; Jones, D.; Heldsinger, D.; Mastrangelo, C. H.; Burke, D. T. Science, 282 (1998) 484-487.

(38) Chabert, M.; Dorfman, K. D.; deCremoux, P.; Roeraade, J.; Viovy, J. L. Analytical Chemistry, 78 (2006) 7722-7728.

(39) Chabert, M.; Viovy, J. L. Proceedings of the National Academy of Sciences, 105 (2008) 3191-3196.

(40) Sugiura, S.; Oda, T.; Izumida, Y.; Aoyagi, Y.; Satake, M.; Ochiai, A.; Ohkohchi, N.; Nakajima, M. Biomaterials, 26 (2005) 3327-3331.

(41) Parsons, L. H.; Justice, J. B. Journal of Neurochemistry, 58 (1992) 212-218.

(42) Robinson, T. E.; Justice, J. B. Journal of Microdialysis in the Neurosciences; Elsevier: Amsterdam, 1991.

(43) Sia, S. K.; Whitesides, G. M. Electrophoresis, 24 (2003) 3563-3576.

(44) Whitesides, G. M.; Ostuni, E.; Takayama, S.; Jiang, X.; Ingber, D. E. Annual Review of Biomedical Engineering, 3 (2001) 335-373.

(45) Anderson, J. R.; Chiu, D. T.; Jackman, R. J.; Cherniavskaya, O.; McDonald, J. C.; Wu, H.; Whitesides, S. H.; Whitesides, G. M. Analytical Chemistry, 72 (2000) 3158-3164.

(46) Duffy, D. C.; McDonald, J. C.; Schueller, O. J. A.; Whitesides, G. M. Analytical Chemistry, 70 (1998) 4974-4984.

(47) McDonald, J. C.; Whitesides, G. M. Accelerated Chemical Research, 35 (2002) 491-499.

(48) Cellar, N. A.; Burns, S. T.; Meiners, J. C.; Chen, H.; Kennedy, R. T. Analytical Chemistry, 77 (2005) 7067-7073.

(49) Zhao, B.; Moore, J. S.; Beebe, D. J. Science, 291 (2001) 1023-1026.

(50) Shackman, J. G.; Watson, C. J.; Kennedy, R. T. Journal of Chromatography A, 1040 (2004) 273-282.

(51) Wilkes, J. O. Fluid Mechanics for Chemical Engineers; Pearson Education, Inc.: Upper Saddle River, NJ, 2006, 414-419.

(52) Culbertson, C. T.; Jacobson, S. C.; Michael Ramsey, J. Talanta, 56 (2002) 365-373.

(53) Paxinos, G.; Watson, C. The Rat Brain in Stereotaxic Coordinates; Academic Press, 1998.

(54) Garstecki, P.; Fuerstman, M. J.; Stone, H. A.; Whitesides, G. M. Lab on a Chip, 6 (2006) 437-446.

(55) Tice, J. D.; Song, H.; Lyon, A. D.; Ismagilov, R. F. Langmuir, 19 (2003) 9127-9133.

(56) Stenken, J. A.; Topp, E. M.; Southard, M. Z.; Lunte, C. E. Analytical Chemistry, 65 (1993) 2324-2328.

(57) Fox, P. T.; Raichle, M. E.; Mintun, M. A.; Dence, C. Science, 241 (1988) 462-464.

(58) Korol, D. L.; Gold, P. E. American Journal of Clinical Nutrition, 67 (1998) 764S-771.

(59) McNay, E. C.; Fries, T. M.; Gold, P. E. Proceeding of the National Academy of Sciences, 97 (2000) 2881-2885.

(60) Hopwood, S. E.; Parkin, M. C.; Bezzina, E. L.; Boutelle, M. G.; Strong, A. J. Journal of Cerebral Blood Flow and Metabolism, 25 (2005) 391-401.

(61) McNay, E. C.; Gold, P. E. Journal of Neurochemistry, 72 (1999) 785-790.

(62) Uehara, T.; Sumiyoshi, T.; Itoh, H.; Kurachi, M. Brain Research, 1133 (2007) 193-199.

(63) Darbin, O.; Carre, E.; Naritoku, D.; Risso, J. J.; Lonjon, M.; Patrylo, P. R. Brain Research, 1116 (2006) 127-131.

APPENDIX B

FINITE ELEMENT METHOD MODELING FLUID DYNAMICS AND MASS TRANSPORT IN AN ADIPOCYTE PERFUSION MICROFLUIDIC DEVICE

1. Context

Many cells are known to respond to the fluidic environment; specifically, adipocytes, or fat cells, undergo low shear stress in natural conditions. At the scale and complex geometry of microfluidic devices, physical parameters such as shear stress are analytically difficult to measure; however, these parameters may be calculated with commercially available finite element method software suites such as COMSOL. In the work described below, both the stress that cells cultured in this devices and the mass transport of gradients to and from the cells were numerically modeled such that they provided good agreement with experimental measures. Specifically, the Reynolds number (R_e) was calculated for the cell chamber, where the diameter of the tube is approximated as $D_H = 4A/P$:

$$R_e = \rho \mathbf{V} D_H / \mu$$

such that at an 80 μL/min flow rate the R_e was well below turbulent conditions (R_e = 5.93e-6) and flow was approximated as Laminar flow. First, the fluid dynamics were solved by setting the outlet pressure to neutral and inlets at a constant flow rate that

summed to 80 μL/min in 3D with a nm mean free path length assuming a rectangular channel with dimensions of 400 by 5000 by 40,000 μm (see Figure B.1). The density and viscosity of water were held constant at 1000 kg/m^3 and 0.001 Pa s, respectively. Shear stress was calculated throughout the chamber and found to be at a maximum value near the walls of the cell channel but with a value of 0.006 N m^{-2} at a probe location near the cells. Second, using the stored values from the fluidic model, convection and diffusion was solved in 3D for a 90 s model with 0.1 s time-steps for the introduction of isoproterenol (D = 1e-9 m^2/s) such that good agreement was found with analytical measures of pumping dyed glycerol into the cell channel. Third, the sampling of glycerol secretions from the cells was modeled. Assuming 1 nanomole of glycerol was secreted for every 10,000 cells and a bed of 50,000 cells per 0.0002 m^2 (average from cell counts after culture), a flux of 4.17e-8 mol/m^2 s was uniformly applied across the bed of the cell channel. Using the literature value for the diffusion of glycerol (D = 7e-10 m^2/s) and fluidic values calculated from the first model, a 1 s pulse, 30 s pulse and constant secretion were modeled for 300 s with 0.1 s time-steps (see Figure B.S1).

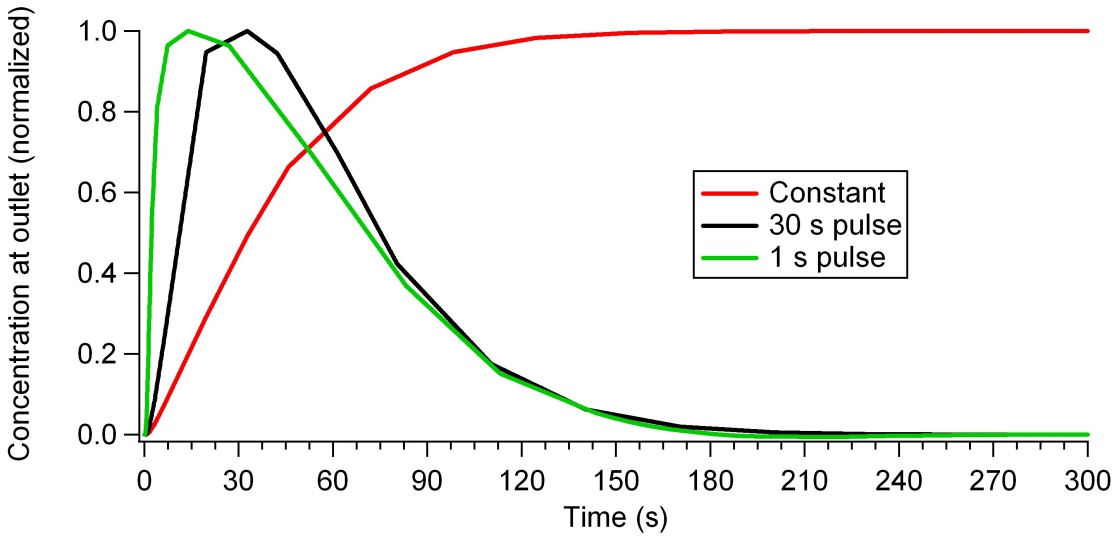

Figure B.S1. Normalized flux of glycerol secretions from a 1 s pulse (green), 30 s pulse (black) and constant release (red) from a packed bed of cells along the bottom of the cell channel.

Moreover, the fluorogenic quantification describe herein was modified from protocol developed for glucose quantification (see Appendix A). The excerpts below were previously published both in Dr A Clark's dissertation and published manuscript ("Continuous-Flow Enzyme Assay on a Microfluidic Chip for Monitoring Glycerol Secretion from Cultured Adipocytes" by Anna M. Clark, Kyle M. Sousa, Colin Jennings, Ormond A. MacDougald, and Robert T. Kennedy in Analytical Chemistry, 81 (2009) 2350-2356):

2. Introduction

Physiological studies frequently require maintaining cells or tissues in a controlled environment while detecting their physical, electrical, or chemical properties. Microfluidics may greatly facilitate such research by allowing creation of highly controlled cell-compatible environments integrated with sophisticated measurement and cell manipulation methods. Examples of using microfluidics for cell physiology include

screening for ligand binding and reporter gene expression from immobilized cells using fluorescence microscopy [1], determining metabolic flux from electrically stimulated cells using amperometry [2], and characterizing drug dose-response using patch clamp methods [3]. Another common physiological method that may benefit from microfluidics is monitoring secretion of chemicals from perfused cells. Without microfluidics, such studies are typically laborious as they require collection and subsequent chemical analysis of large numbers of fractions. Microfluidics may improve perfusion and secretion measurements by reducing costs through reduction of reagent usage, allowing automated analysis, reducing cells required, improving throughput, allowing novel perfusion patterns, and improving temporal resolution [4-6].

Several examples of using chips to monitor cellular secretions have been reported [7-13]. These include using electrophoretic immunoassay to measure insulin secretion from islets of Langerhans [7-8], amperometry to monitor catecholamine release from PC12 cells [9], and chemiluminescence to detect glucose and ethanol secretions from *S. cerevisiae* [10]. Enzyme assays have also proven to be a viable approach to monitoring cellular secretions on microfluidic devices. Enzyme assays have been utilized on microfluidic devices to study metabolic secretions from preimplantation embryos [11], activity of expressed enzymes from *E. coli* cells [12], and immune response from macrophages [13].

In this study, we extend such measurements to near real-time monitoring of glycerol secretion from an adipocyte cell line (differentiated murine 3T3-L1 cells) [14-15] using a continuous-flow enzyme assay. The prevalence of obesity and obesity-related disorders underscores the necessity to study and to understand adipocyte

physiology. A primary function of adipocytes is to store and release energy. Adipocytes store energy as triacylglycerol and release fatty acids and glycerol by lipolysis to supply energy for other tissues and organs. Measurement of glycerol secretion is often used to ascertain the function and physiological state of adipocytes [16-19]. Studying adipocytes in microfluidic devices is hampered by several fat cell properties including high buoyancy, lengthy culture times (~2 weeks) to differentiate adipocyte cell lines, fragility of lipid-laden adipocytes, and secretion of hydrophobic moieties which are difficult to transport through PDMS-based devices. Despite these difficulties, adipocytes have been differentiated [20-21], studied for incorporation of toxins [20, 22], and examined for size [23] on chips; however, integration of cultured adipocytes with chemical measurement of cellular secretions has yet to be performed.

We have developed a dual-chip microfluidic system for culturing adipocytes, perfusing them, and then monitoring glycerol release using a continuous-flow fluorescent enzyme assay. One chip was a cell perfusion chamber. Cells grown on conventional cover slips could be loaded into the reversibly-sealed chip for perfusion experiments. These features allowed the chip to be reused and allowed cells to be cultured for long periods in conventional incubators prior to use. The second chip was used for continuous-flow enzyme assay. To achieve sufficient sensitivity, a commercially available absorbance-based enzyme assay for glycerol was converted to a fluorescence-based enzyme assay by the inclusion of the hydrogen peroxide-sensitive dye Amplex UltraRed. For actual measurements, the chips were coupled so that effluent from the perfusion chip was transferred to the enzyme assay chip allowing adipocyte secretions to be monitored on-line with 90 s temporal resolution. The system was used to demonstrate

transient increases in glycerol secretion during exposure of the cells to isoproterenol, a β-adrenergic agonist. The ability to modify enzyme assays for fluorescence-based detection and analyze cells grown in culture on cover slips demonstrates the potential to monitor metabolite secretions in real-time from various cell types utilizing the microfluidic system presented.

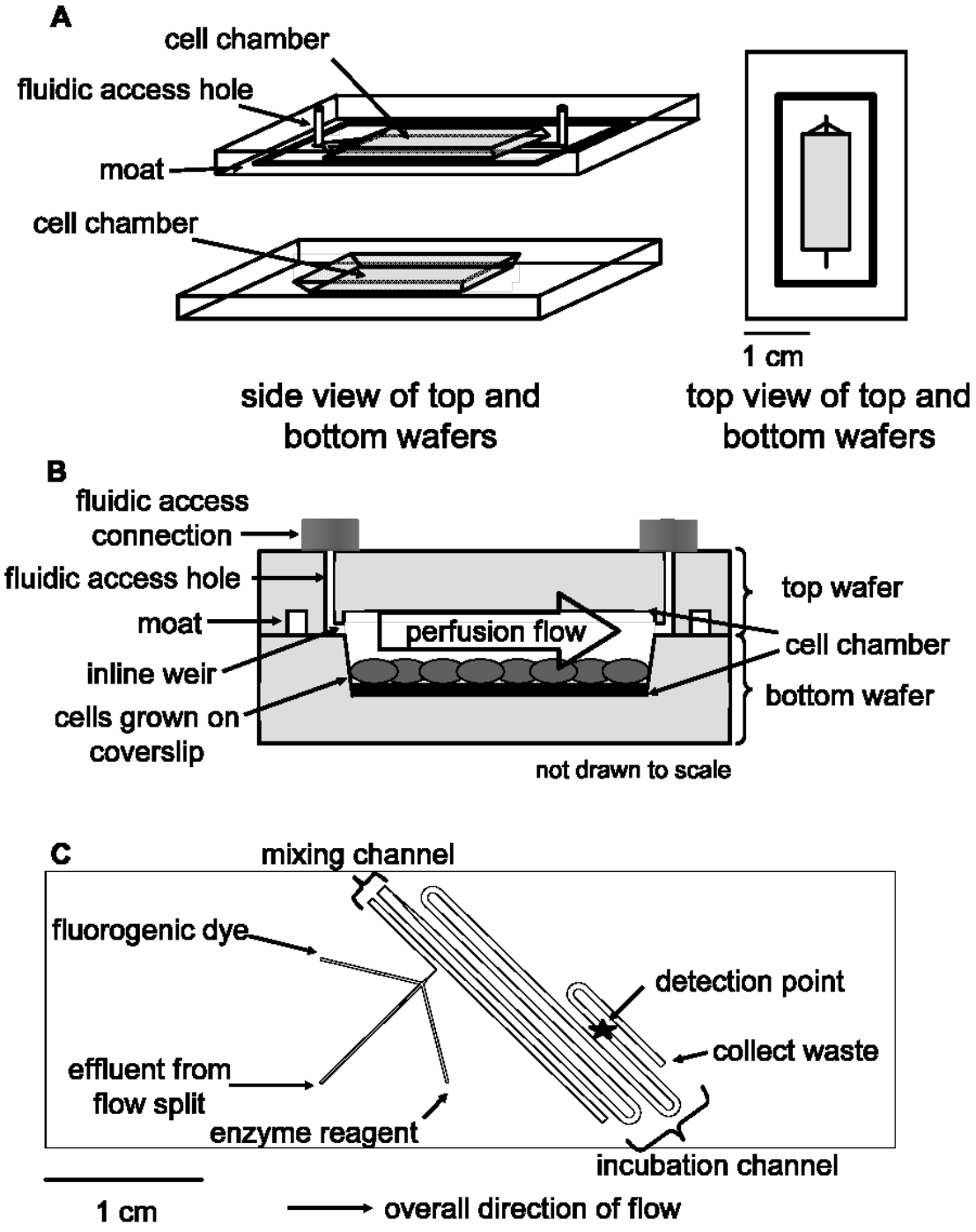

Figure B.1. Schematics of the two microfluidic devices used in this work. (a) A diagram of the perfusion cell chip depicts the two separate wafers employed in this work. The wafers were reversibly sealed with the aid of an in-house built compression frame. (b) A side view of the perfusion chip displays the cell chamber, which contained 50 000 differentiated adipocytes. Perfusion solution washed over the cells to sample secretions released from the cells. (c) The enzyme assay chip was capable of performing on-line

mixing of three solutions and on-line detection of the enzymatic product. The layout shows the initial mixing channel connected to the incubation channel.

3. Materials and Methods

3.1 Chemicals and Reagents

Free glycerol reagent, glycerol standard solution, isoproterenol, dimethyl sulfoxide (DMSO), cell culture reagents, and 1x Hanks balanced salt solution (HBSS) were purchased from Sigma (St. Louis, MO). Amplex UltraRed was purchased from Invitrogen (Carlsbad, CA). All other chemicals were purchased from Fisher (Pittsburgh, PA). Glycerol standards and the glucose solution perfused over cells were made using HBSS as solvent. All other solutions were made using Milli-Q (Millipore, Bedford, MA) 18-MΩ deionized water. Solutions perfused through microfluidic devices were filtered using 0.2-μm nylon syringe filters (Fisher).

3.2 Computational Modeling of Perfusion Chip

The fluid flow dynamics of the perfusion cell chip were modeled using COMSOL Multiphysics 3.3 (Comsol, Inc., Burlington, MA). The flow was defined to be laminar and with a volumetric flow rate of 80 μL min^{-1}. Constants used in the model were 1×10^{-9} m^2 s^{-1} as diffusion coefficient for glycerol, 6.85×10^{-10} m^2 s^{-1} as diffusion coefficient for isoproterenol, 993 kg m^{-3} for density of water, and 6.90×10^{-4} Pa s for viscosity of water (37 °C). The cell chamber volume used was 4 cm long, 0.5 cm wide, and 0.04 cm deep (0.01 cm from the top wafer and 0.03 cm from the bottom wafer after accounting for the presence of the 0.015 cm thick cover slip).

3.3 Enzymatic Assay and On-line Mixing

A commercially available absorbance-based, enzyme assay (Free Glycerol Reagent, Sigma) for glycerol was converted to fluorescence-based detection by the inclusion of the hydrogen peroxide sensitive dye Amplex UltraRed resulting in the assay scheme shown in Figure B.2A. Amplex UltraRed was diluted with DMSO to result in a 100 μM solution upon on-chip mixing. The glycerol enzyme reagent was reconstituted according to manufacturer's instructors. The enzyme reagent, which contained all necessary enzymes and co-factors, was mixed with dye and sample and allowed to react for 5 min prior to detection.

To perform this assay on the microfluidic enzyme chip (Figure B.1C), sample or perfusate from the perfusion chip was transferred via capillary to the enzyme assay chip as a continuous flow. The flow was split so that only 0.31% of the flow from the perfusion chip entered the enzyme chip with the rest going to waste. The flow split was achieved using a Valco tee between the chips with the following capillary lengths and inner diameters for connection: 20 cm, 150 μm from perfusion chip to flow split; 10 cm, 50 μm from flow split to enzyme chip; 7 cm, 150 μm from flow split to waste. All capillary outer diameters were 360 μm. The enzyme reagent and fluorogenic dye were each delivered to the enzyme assay chip via capillary (40 cm, 50 μm i.d.) by a syringe pump (model 402, CMA Microdialysis, North Chelmsford, MA) fitted with 100 μL Hamilton syringes (Reno, NV) resulting in a 1:1:1 ratio of solutions. The inlet flows from each of the 3 channels were 250 nL min^{-1} each resulting in a total volumetric flow rate through the device of 750 nL min^{-1}. The merged streams flowed into a 7.1 cm long mixing channel (90 μm width at half-height), which was kept relatively narrow to

facilitate mixing, and then a 3.75 cm long incubation channel (648 μm width at half-height). The latter channel was wider to reduce the pressure required for pumping. All enzyme assay chip channels were etched to a depth of 60 μm. The combined lengths allowed a 5 min mixing and incubation time.

4. Results and Discussion

4.1 On-line Enzyme Assay Characterization

To characterize the response of the system, glycerol standards were pumped through the cell perfusion chip and into the enzyme assay chip where they were mixed with reagents for the glycerol assay, while monitoring fluorescence (Figure B.2B). For this experiment, glycerol standards were pumped through the perfusion chip at 80 μL min^{-1}. The LOD of the on-line fluorescence-based enzyme assay, determined by the concentration that gave a signal 3 times the standard deviation of the blank, was 4 μM for glycerol. The assay gave a linear response from the detection limit to 50 μM glycerol (Figure B.2C). RSDs were from 1-5% indicative of a stable reaction and efficient mixing of the reagents. The signal generated by the fluorescence-based glycerol assay yielded similar RSDs over 3 h for both the blank and a 25 μM glycerol standard, typical basal concentration of glycerol detected from mature adipocytes, indicating good stability and relatively long term operation. Day-to-day reproducibility of the calibration was good with slope equal to 1105 ± 56 RFU μM^{-1} and intercept 9329 ± 1658 RFU (n = 6).

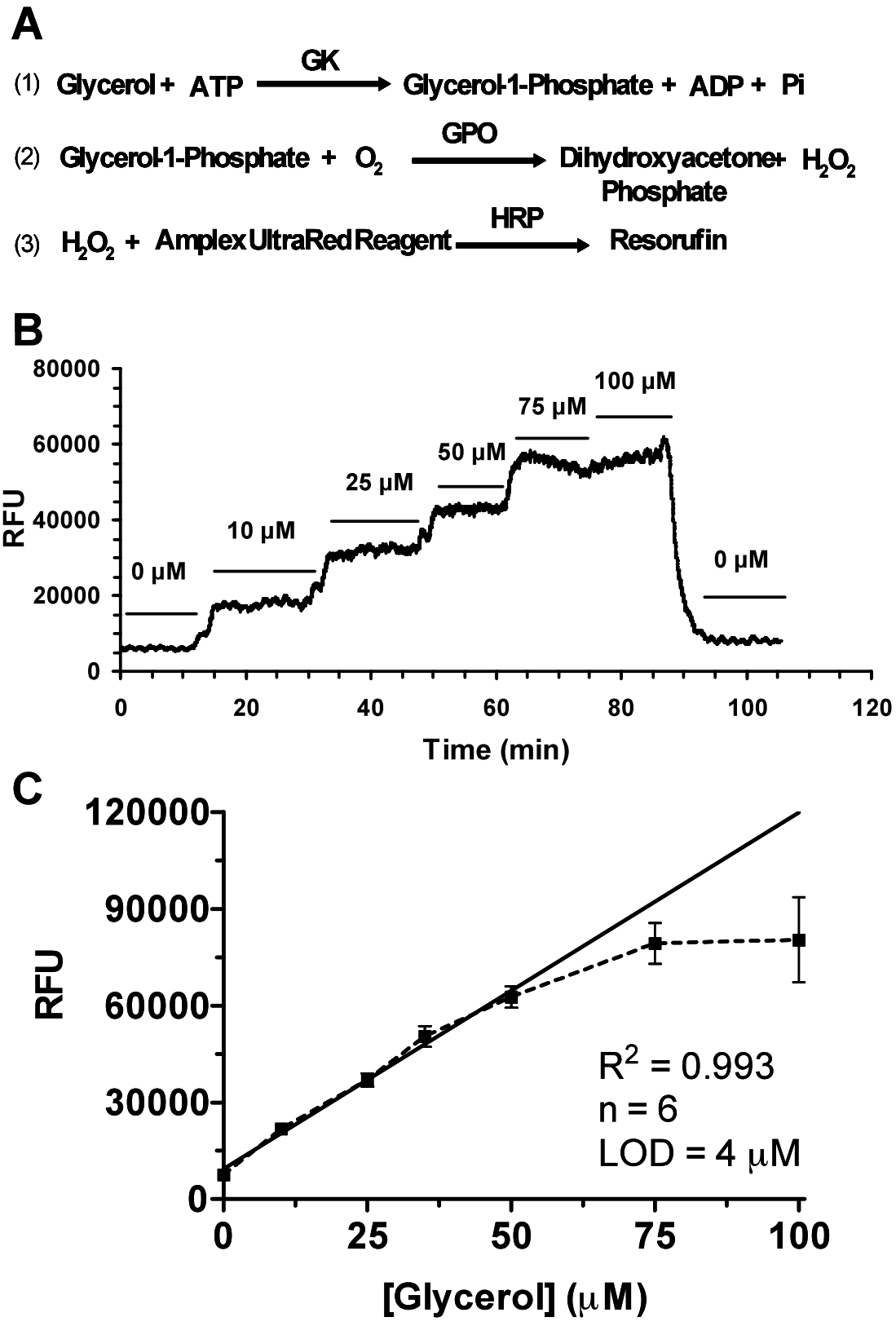
A
(1) Glycerol + ATP GK Glycerol-1-Phosphate + ADP + Pi
(2) Glycerol-1-Phosphate + O2 GPO Dihydroxyacetone Phosphate + H2O2
(3) H2O2 + Amplex UltraRed Reagent HRP Resorufin
B
RFU
Time (min)
0 µM
10 µM
25 µM
50 µM
75 µM
100 µM
0 µM
C
RFU
[Glycerol] (µM)
R2 = 0.993
n = 6
LOD = 4 µM

Figure B.2. Characterization of on-line fluorescence-based enzyme assay. (a) The scheme of the fluorescence-based enzyme assay for glycerol employed for on-chip mixing and detection is depicted. Glycerol kinase (GK), glycerol phosphate oxidase (GPO), peroxidase (HRP), and Amplex UltraRed were mixed on-chip with glycerol (either from standards or cell effluent) to form the fluorescent product resorufin. (b) An example step-change calibration utilizing the dual-chip system is shown. Glycerol concentrations ranging between 0-100 μM were perfused through the system to determine the corresponding changes in fluorescence. (c) The overall calibration generated a LOD of 4 μM and was linear from 0-50 μM glycerol.

The rise time of the system, as determined by a 10-90% change in signal for a step-change in glycerol concentration, was 90 s. If the cell perfusion chip was by-passed, the rise time improved to 80 s. Little change in rise time was observed at various points along the incubation channel of the enzyme chip. These observations combined indicate that the greatest source of dispersion was due to the fluidic connections such as the connection volumes and transfer capillaries, not the incubation time or the cell chip.

4.2 Glycerol Secretion from Adipocytes

To test the system for monitoring dynamic changes in glycerol release from adipocytes, we monitored glycerol secretion during treatment of adipocytes with the β-adrenergic agonist isoproterenol, which is known to elevate cellular cAMP, activate protein kinase A and stimulate lipolysis [27]. For these experiments, cells were loaded into the cell chamber and perfused with glucose-HBSS while monitoring the enzyme reaction as described above for the standards. The cells remained adherent during transfer and perfusion. Basal measurements were collected for at least 60 min and yielded an average concentration of 28 $\pm$ 5 μM (SEM, n = 5). Upon switching to a

perfusion fluid containing 20 μM isoproterenol, a transient burst of glycerol secretion of approximately 3-fold over basal secretion was detected followed by a sustained release that was ~40% over basal levels (see Figure 3 for sample individual traces and averaged responses). The burst in glycerol release rose within the first 2 min of exposure to isoproterenol and decreased after ~6 min. The cell system gave stable responses allowing glycerol secretion to be monitored for at least 3.5 h, although most experiments were completed in 2 h.

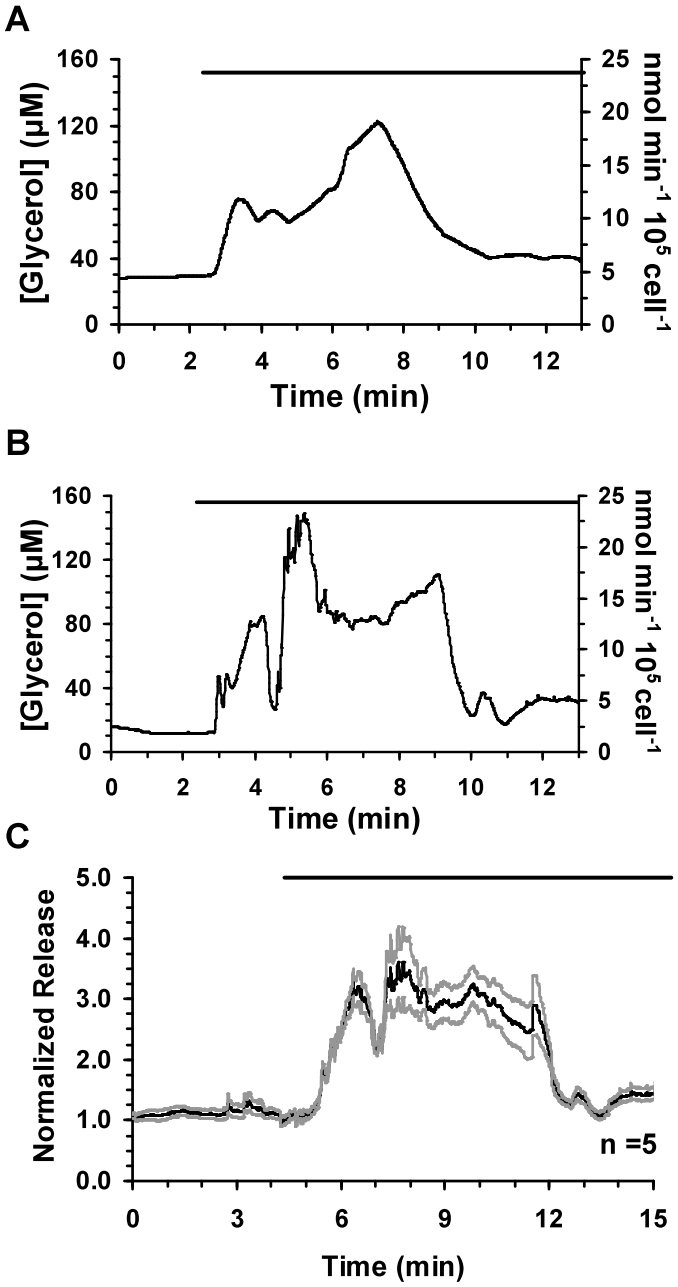

Figure B.3. Glycerol secretion data from differentiated adipocytes and response to isoproterenol treatment. (a, b) Representative traces of glycerol release from differentiated adipocytes and response upon 20 μM isoproterenol treatment are shown. (c) Five glycerol secretion traces were averaged and shown with ± SEM. The SEM above and below the average was plotted to enable visualization of the error between measurements. The bars above traces represent exposure to 20 μM isoproterenol. The traces were shortened to depict only the time surrounding the initial exposure to isoproterenol.

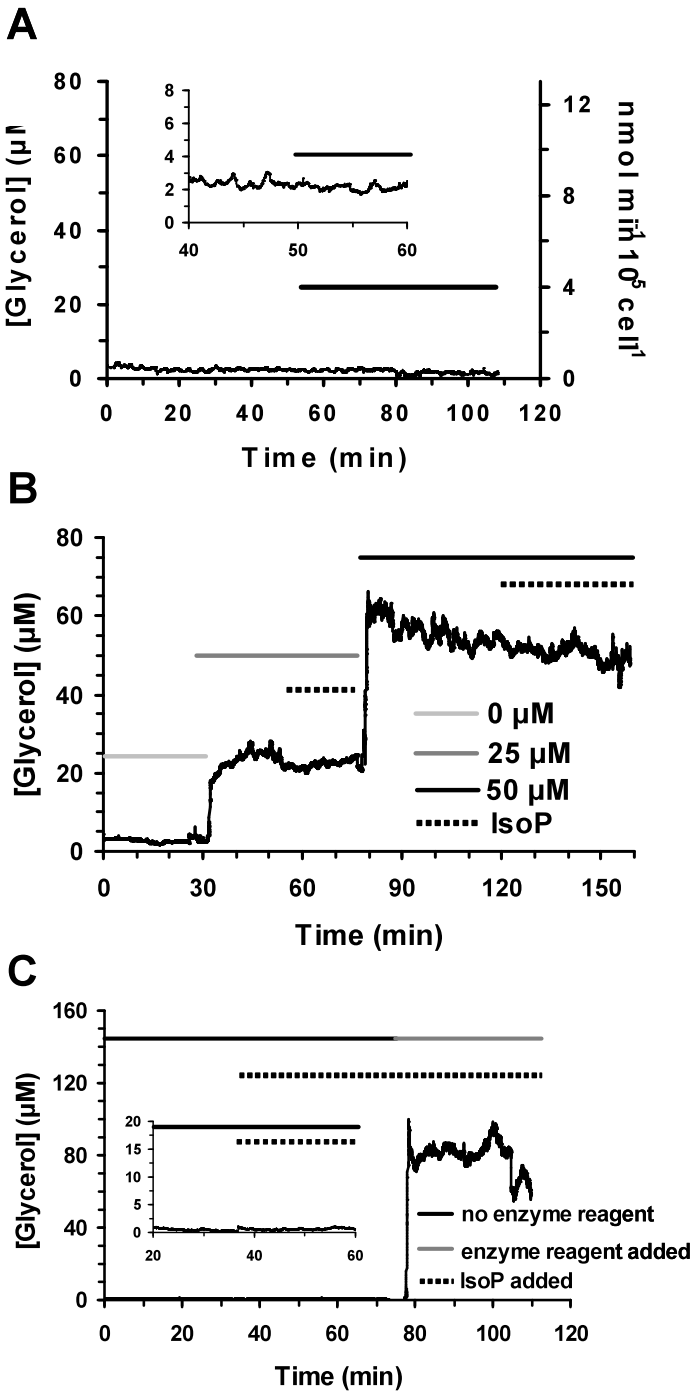

Figure B.4. Control secretion data. (a) Glycerol secretion data was obtained from 95% confluent preadipocytes. The bar indicates perfusion of 20 µM isoproterenol. The y-axis of the insert is 10x greater to enable visualization of the glycerol release measured. (b) The effect of isoproterenol introduction on the on-line enzyme assay was determined to be minimal at both 25 µM and 50 µM glycerol. The light grey line

indicates perfusion of 0 μM glycerol standard, medium grey 25 μM, and black 50 μM, respectively. The dashed line represents exposure to 20 μM isoproterenol. (c) The response of the system without the enzyme reagent present and upon inclusion of the enzyme reagent during a cellular secretion experiment was tested. The black and grey lines represent the absence and presence of the enzyme reagent, respectively. The dashed line represents treatment with 20 μM isoproterenol. The y-axis scale of the insert is 8x greater for visualization of the release monitored when isoproterenol was introduced in the absence of the enzyme reagent.

In several experiments, fractions were collected from the waste capillary and analyzed for glycerol using the standard assay yielded glycerol concentrations. These experiments yielded glycerol concentrations that on average were with 6% of the on-line measurement (n = 10 fractions from 4 experiments). Moreover, Getty-Kaushik and colleagues reported an increase in overall glycerol secretion upon perfusion of primary rat adipocytes with isoproterenol [17]. These results indicate the reliability of the on-line measurements.

4.3 Characterization of Cell Perfusion Chip

We also characterized the perfusion chip with simulations and experiments to determine the shear stress on cells and uniformity of drug application to the cells. Due to the fragility of adipocytes, the perfusion chip was designed to have a recessed cell chamber area relative to the inlet and outlet flow stream to reduce shear stress and permit laminar flow of fluid over the cells. This design was inspired by previous work that showed that shear force is diminished by placing the fluid inlet above the cells and not inline with them [28]. The COMSOL model of our chip estimated the shear stress upon

the cells at 0.006 N m^{-2}. This value is in the same range as reported in other microfluidic systems employing cell perfusion [5] despite the high volumetric flow rate employed. This low value, plus the observation that the flow did not cause cells to detach or deform, suggests that the chip design prevents excessive shear on the cells.

A potential concern with this design is that drugs are not uniformly applied to the cells. To test for uniformity of flow across the width of the cell chamber, food dye was flowed into the perfusion chip to visualize the flow profile. Pictures of the flow showed that fluid flow was dispersed evenly across the width of the chip, an observation confirmed by COMSOL modeling. This study also confirmed that: 1) the solution stays confined to the cell chamber, i.e., it does not leak past the moat, 2) the chip washes out rapidly, and 3) flow exhibits the characteristic parabolic profile of laminar flow. To determine if drugs applied would uniformly reach the bottom of the chip, we used a COMSOL model because of the difficulty of directly imaging the depth of penetration of dyes. The model predicted that fluid flowed throughout the entire depth of the cell chamber region and that substances in the perfusion flow, such as isoproterenol, would rapidly reach a uniform concentration throughout the depth of the chip due to a combination of flow and diffusion. Washout of the cell chamber using the model was predicted to occur in 55 s, which closely matched the observed washout time of 60 s and further validated the efficacy of the model.

The results show that the dual-chip system is a useful approach to adipocyte culture and monitoring. Although an integrated chip would likely result in a better temporal response by reducing the connection volume between the cells and assay, the dual chip platform allowed both components of the system, cell perfusion and enzyme

assay, to be optimized separately. The two-chip approach also had other practical advantages including: 1) ability to operate the perfusion chip while inverted if necessary to prevent cells floating in the direct flow stream without affecting detection in the assay chip (floating cells being a more likely problem with primary adipocytes), and 2) compatibility of a reversibly sealed chip, useful for cell loading, and a bonded chip, useful for enzyme assay.

The perfusion chip was designed to overcome challenges associated with coupling adipocytes with microfluidic devices. Glass was chosen as the material for the microfluidic chips as adipocytes secrete hydrophobic moieties that may interact with or adhere to polymeric materials. The inline weir at the inlet and exit of the chip (Fig. 1B), created through multi-step etching, confined the cells to the cell chamber area and prevented cells from creating clogs in downstream channels as adipocytes may become non-adherent and float. The inlet and outlet locations also minimized shear stress on the cells while allowing drugs to be uniformly and quantitatively applied. To circumvent the long culture time, murine 3T3-L1 adipocytes were grown on glass cover slips that could be placed into the perfusion chip for experiments. Growing cells on cover slips had numerous advantages including: 1) enabling growth of the cells in Petri dishes according to previously optimized culture conditions, 2) increased throughput for secretion experiments relative to growing cells directly in the cell chamber, 3) decreased variability of measurements as multiple cover slips could be tested from the same Petri dish of cells, and 4) potential to return cells to culture following an experiment for re-use. Furthermore, testing cultured cells in a resealable chip enabled the same device to be used numerous times. Indeed, the same chips were used for the entirety of the

experiments presented in this paper (data collected over the course of 6 months). The robustness of the chip increases the convenience of use and negates the cost disadvantage of working with glass as the chip material.

Coupling the perfusion chip with the on-line enzyme assay proved efficacious for monitoring cellular activity. Transient secretion dynamics from adipocytes were able to be observed upon treatment with isoproterenol. The sharp rise in glycerol release within the first two minutes of exposure to isoproterenol likely reflects the fast signaling associated with phosphorylation and activation of hormone sensitive lipase and other proteins involved in lipolysis. The decrease in secreted levels after ~6 min may be due to internalization of the β-adrenergic receptor and pathway desensitization upon continuous perfusion of ligand. Previous work with primary rat adipocytes also has shown a burst in glycerol secretion in response to isoproterenol treatment as well as sustained, elevated release [17]. The duration of the pulse was ~3 times longer with primary rat adipocytes compared to the pulse detected in this work using immortalized 3T3-L1 adipocytes. However, a similar increase in overall glycerol levels upon treatment with isoproterenol was reported. In this work, the secretion data also consistently showed two peaks during this initial burst of glycerol release. This effect needs further study but may reflect internal dynamics such as mobilization of triacylglycerol stores.

While adipocyte secretions have previously been monitored off-line fraction collection [16-19], this microfluidic-based platform facilitates automated mixing and detection to greatly save on labor and reagent costs. Compared to the same experiments performed using off-line assays, i.e. following the manufacturer's instructions and using an equivalent concentration of fluorogenic dye with readout on a plate reader, the chip

system employing the on-line enzyme assay consumed less than 1% Amplex UltraRed and less than 0.05% enzyme reagent (i.e., 800 μL per aliquot of enzyme reagent is consumed off-line with effluent fractions collected every min compared to 250 nL min^{-1} on-line). Additionally, the on-line format diminished labor by removing numerous pipetting steps resulting in shorter analysis time. This work also complements other work, such as use of calorimetry for monitoring adipocyte function on chips [29]. The fluorescence assay offers specific chemical detection while the calorimetry method offers an overview of cell metabolism.

5. Conclusions

We developed a microfluidic platform consisting of two separate chips to integrate cell perfusion, sample handling, and reagent mixing as well as to enable near real-time monitoring of glycerol release from cultured adipocytes. The microfluidic platform was able to detect changes in glycerol levels from ~50,000 adipocytes under basal conditions and upon pharmacological treatment with isoproterenol. The use of a microfluidic device for on-line mixing and detection reduced the consumption of costly reagents to less than 1% of off-line volumes and decreased labor by automating the mixing and detection on-chip. Culturing adipocytes on cover slips increased the throughput of cells available for study as well as decreased biological variability as multiple experiments could be tested from cells cultured in the original Petri dish. This device may be applied to studying the oscillatory nature of glycerol release and long-term changes in metabolism. While the device has been employed to monitor glycerol secretion from 3T3-L1 adipocytes, it is possible that it can be configured to detect other

moieties secreted by adipocytes such as non-esterified fatty acids, to test primary adipocytes that have been genetically modified and/or exposed to pharmacological treatment, or to monitor secretions from other adherent cell types such as osteoblasts.

References

(1) Davidsson, R.; Boketoft, A.; Bristulf, J.; Kotarsky, K.; Olde, B.; Owman, C.; Bengtsson, M.; Laurell, T.; Emneus, J. Analytica. Chemistry, 76 (2004) 4715-4720.

(2) Cheng, W.; Klauke, N.; Sedgwick, H.; Smith, G. L.; Cooper, J. M. Lab on a Chip, 6 (2006) 1424-1431.

(3) Lau, A. Y.; Hung, P. J.; Wu, A. R.; Lee, L. P. Lab on a Chip, 6 (2006) 1510-1515.

(4) El-Ali, J.; Sorger, P. K.; Jensen, K. F. Nature, 442 (2006) 403-411.

(5) Kim, L.; Toh, Y.-C.; Voldman, J.; Yu, H. Lab on a Chip, 7 (2007) 681-694.

(6) Meyvantsson, I.; Beebe, D. J. Annual Review of Analytical Chemistry, 1 (2008) 423–449.

(7) Roper, M. G., Shackman, J.G., Dahlgren, G.M., Kennedy, R.T. Analytical Chemistry, 75 (2003) 4711-4717.

(8) Shackman, J. G., Dahlgren, G.M., Peters, J.L., Kennedy, R.T. Lab on a Chip, 5 (2005) 56-63.

(9) Li, M. W.; Dana M Spence, D. M.; Martin, R. S. Journal of Electroanalytical Chemistry, 17 (2005) 1171-1180.

(10) Davidsson, R.; Johansson, B.; Passoth, V.; Bengtsson, M.; Laurell, T.; Emnéus, J. Lab on a Chip, 4 (2004) 488-494.

(11) Urbanski, J. P.; Johnson, M. T.; Craig, D. D.; Potter, D. L.; Gardner, D. K.; Thorsen, T. Analytical Chemistry, 80 (2008) 6500-6507.

(12) Huebner, A.; Olguin, L. F.; Bratton, D.; Whyte, G.; Huck, W. T. S.; de Mello, A. J.; Edel, J. B.; Abell, C.; Hollfelder, F. Analytical Chemistry, 80 (2008) 3890-3896.

(13) Goto, M.; Sato, K.; Murakami, A.; Tokeshi, M.; Kitamori, T. Analytical Chemistry, 77 (2005) 2125-2131.

(14) Kawamura, M.; Jensen, D. F.; Wancewicz, E. V.; Joy, L. L.; Khoo, J. C.; Steinberg, D. Proceedings of the National Academy of Sciences, 78 (1981) 732-736.

(15) Rosen, E. D.; Spiegelman, B. M. Annual Review of Cellular Biology, 16 (2000) 145-171.

(16) Getty, L.; Corkey, B. Diabetes, 52 (2003) A82-A82.

(17) Getty-Kaushik, L., Richard, A-M.T., Corkey, B.E. Diabetes, 54 (2005) 629-637.

(18) Getty-Kaushik, L.; Richard, A.-M. T.; Corkey, B. E. Obesity Research, 13 (2005) 2058-2065.

(19) Getty-Kaushik, L.; Song, D. H.; Boylan, M. O.; Corkey, B. E.; Wolfe, M. M. Obesity, 14 (2006) 1124-1131.

(20) Viravaidya, K., Shuler, M.L. Biotechnology Progress, 20 (2004) 590-597.

(21) Ni, X. F., Crozatier, C., Sensebé, L., Langonne, A., Wang, L., Fan, Y., He, P.G., Chen, Y. Microelectronic Engineering, 85 (2008) 1330-1333.

(22) Nakayama, H., Kimura, H., Komori, K., Fujiii, T., Sakai, Y. AATEX, 14 (2007) 619-622.

(23) Wang, H.-W., Bao, N., Le, T.T., Lu, C., Cheng, J-X. Optics Express, 16 (2008) 5782-5789.

(24) El-Jack, A. K., Hamm, J.K., Pilch, P.F., and Farmer, S.R. Journal of Biological Chemistry, 274 (1999) 7946-7951.

(25) Ross, S. E., Hemati, N., Longo, K.A., Bennett, C.N., Lucas, P.C., Erickson, R.L., MacDougald, O.A. Science, 289 (2000) 950-953.

(26) Shackman, J. G., Watson, C.J., Kennedy, R.T. Journal of Chromatography A, 1040 (2004) 273-282.

(27) Arner, P. Best Practices in Clinical Research, 19 (2005) 471-482.

(28) Figallo, E.; Cannizzaro, C.; Gerecht, S.; Burdick, J. A.; Langer, R.; Elvassore, N.; Vunjak-Novakovic, G. Lab on a Chip, 7 (2007) 710-719.

(29) Johannessen, E. A.; Weaver, J. M. R.; Bourova, L.; Svoboda, P.; Cobbold, P. H.; Cooper, J. M. Analytical Chemistry, 74 (2002) 2190-2197.